Zn/Fe systematics in mafic and ultramafic systems: Implications for detecting major element heterogeneities in the Earth's mantle

V. Le Roux *, C.-T.A. Lee, S.J. Turner [1]

Department of Earth Sciences, Rice University, MS-126, 6100 Main Street, Houston, TX 77005, USA

Received 10 September 2009; accepted in revised form 3 February 2010; available online 10 February 2010

Abstract

Oceanic basalts, such as mid-ocean ridge basalts (MORB) and ocean island basalts (OIB), are characterized by large isotopic and trace element variability that is hard to reconcile with partial melting of a peridotitic mantle alone. Their variability has been attributed to the presence of heterogeneities within the mantle, such as recycled crust, metasomatized material or outer core contribution. There have been few attempts to constrain the major element composition of those heterogeneities, most studies focusing on incompatible trace elements and radiogenic isotopes. Here, we report Zn, Mn and Fe systematics in mafic and ultramafic systems (whole-rocks and minerals) and we explore their use for detecting lithological heterogeneities that deviate from peridotitic mantle dominated by olivine and orthopyroxene. We suggest that Zn/Fe ratio is a particularly promising proxy. Zn/Fe fractionates equally between olivine, orthopyroxene and melt (e.g. the inter-mineral exchange coefficients $K_{D(\text{Ol/melt})}^{\text{Zn/Fe}} \sim K_{D(\text{Opx/melt})}^{\text{Zn/Fe}}$ is $\sim$0.9–1), and the distribution of Zn/Fe between minerals appears to be temperature-independent within error. In contrast, clinopyroxene and garnet are characterized by low Zn/Fe ratios compared to co-existing melt, olivine and orthopyroxene, that is, $K_{D(\text{Cpx/melt})}^{\text{Zn/Fe}}$ and $K_{D(\text{Gt/melt})}^{\text{Zn/Fe}}$ are both $\ll 1$. These partitioning behaviors imply that Zn/Fe ratios are minimally fractionated during partial melting of peridotite and differentiation of primitive basalts, if differentiation is dominated by olivine control. Thus, the Zn/Fe ratios of primitive basalts preserve the Zn/Fe ratio of the primary parental magma, providing insight into the signature of the mantle source region. We also infer that Zn/Fe ratios in melts are unlikely to be fractionated by modal variations in peridotitic material but are highly fractionated if garnet and/or clinopyroxene are the main phases in the source during melting. Similar Zn/Fe ratios between MORB and average upper mantle confirm the lack of fractionation during peridotite melting. However, high Zn/Fe ratios of some OIB cannot be explained by peridotite melting alone, but instead require the presence of high Zn/Fe lithologies or lithologies that have bulk exchange coefficients $K_{D(\text{rock/melt})}^{\text{Zn/Fe}} < 1$. All garnet-bearing or clinopyroxene-bearing lithologies, such as eclogites and garnet pyroxenites, fit the latter requirement.

© 2010 Elsevier Ltd. All rights reserved.

1. INTRODUCTION

Over the last decade, a number of studies have shown that oceanic basalts are highly variable in their isotopic and trace element signatures, suggesting the presence of both enriched and depleted components in the Earth's mantle (e.g. Hofmann and White, 1982; Zindler and Hart, 1986; Hauri, 1996; Lassiter and Hauri, 1998). Several hypotheses have emerged on the nature and the distribution of these components. It has been proposed that the source of mid-ocean ridge basalts (MORB) contains a recycled crustal component (Hirschmann and Stolper, 1996; Eiler et al., 2000; Salters and Dick, 2002; Sobolev et al., 2007) and that ocean island basalts (OIB) carry the signature of garnet pyroxenites (e.g. Allegre and Turcotte, 1986; Hirschmann et al., 2003; Prytulak and Elliott, 2007; Sobolev et al., 2007; Dasgupta et al., 2010), of metasomatized lithosphere

---

* Corresponding author. Tel.: +1 281 796 7718.
  E-mail address: veronique.leroux@rice.edu (V. Le Roux).
[1] Present address: Department of Earth and Planetary Sciences, Harvard University, 20 Oxford Street, Cambridge, MA 02138, USA.

(e.g. Pilet et al., 2008 and references therein), or of an outer core contribution (Walker et al., 1995; Brandon et al., 1999; Humayun et al., 2004). As a result, there is no consensus on the nature and spatial distribution of mantle heterogeneities. Even less is known about the extent and nature of major element or lithological heterogeneities because most of the geochemical tracers so far have focused on isotope and trace element systems. Only recent studies have started to tackle the problem of major element heterogeneities (e.g. Sobolev et al., 2005, 2007; Jackson and Dasgupta, 2008; Dasgupta et al., 2010).

Understanding the extent of major element heterogeneities in the mantle is a key question because major elements dictate mantle mineralogy, temperature of melting and physical properties such as density and viscosity. The stakes are high because petrologic estimates of mantle temperature based on primitive magmas assume that the composition of the mantle source is that of canonical primitive mantle (e.g. pyrolite-like composition with $Mg\# = molar\ Mg/(Mg + Fe) \sim 0.89–0.9$; Green et al., 1979; Jagoutz et al., 1979; Sun, 1982). If, in some places, the mantle's major element composition differs from peridotitic mantle then errors in temperature estimation arise. For instance, if we assume that olivine is the main phase in the source and its forsterite content is Fo_{90}, mantle temperatures may be over-estimated if Fe-rich heterogeneities are neglected (Roeder and Emslie, 1970; Putirka, 2005).

Little is known about major element variability at depth because we have a limited view of the Earth's mantle. First, peridotite xenoliths only sample parts of the lithospheric mantle, while tectonically-emplaced mantle rocks outcrop only in specific geological settings. Moreover, many of these rocks may have been refertilized, impregnated and/or cryptically metasomatized, thus modifying compositional trends associated with partial melting (e.g. Rampone et al., 1997; Muntener et al., 2004; Le Roux et al., 2007). Second, our view of mantle heterogeneity comes mainly from trace elements and radiogenic isotope systems (Hofmann, 1997). Because they are usually highly incompatible in solids and hence enriched in melts and fluids, trace elements and isotope systems based on incompatible elements are particularly affected by cryptic metasomatism, decoupling these systems from major elements. Lastly, major element abundances in mantle-derived magmas are controlled by the cumulated effects of source composition, pressure and temperature conditions of melting, fractional crystallization and crustal assimilation. Thus, the major element composition of evolved magmas may no longer be representative of their mantle source.

The purpose of this paper is to identify geochemical proxies that show minimal solid–melt fractionation during peridotite melting but are sensitive to melting of non-peridotitic lithologies. To avoid some of the problems discussed above, our approach here is to use ratios of trace elements and major elements that are only moderately incompatible during melting of typical peridotite and remain relatively unfractionated during early magmatic differentiation. Because olivine and orthopyroxene are the major phases in peridotites, the ideal elemental ratio would be one that is primarily controlled but not fractionated by olivine and orthopyroxene and yet fractionated when other minerals, such as garnet and clinopyroxene, are the dominant phases during melting. More specifically, we can express the degree to which an elemental ratio, e.g. A/B, fractionates by the exchange coefficient between two phases i and j (which could be minerals or melt), that is,

$$K_{D(i/j)}^{A/B} = \frac{(A/B)_i}{(A/B)_j} \tag{1}$$

For instance, the well-known olivine/melt $K_{D(Ol/melt)}^{Fe/Mg}$ of ~ 0.3 for Fe–Mg exchange is given by $K_{D(Ol/melt)}^{Fe/Mg} = \frac{(Fe/Mg)_{Ol}}{(Fe/Mg)_{melt}}$, where Fe strictly speaking refers only to Fe^{2+} (Roeder and Emslie, 1970). The ideal elemental ratio would have $K_{D(Ol/melt)}$ and $K_{D(Opx/melt)} = 1$ as such a ratio would remain unfractionated from a peridotite source and during olivine-controlled fractional crystallization. Fe/Mg ratios obviously do not fit our demands, but the first series transition metals offer some possibilities because these elements are all moderately incompatible (Canil, 2004). For instance, Fe/Mn has been used as a proxy for source heterogeneities in oceanic basalts (Humayun et al., 2004; Sobolev et al., 2007; Qin and Humayun, 2008) because it is minimally fractionated during partial melting and olivine fractionation (Ruzicka et al., 2001). We will show below that Zn/Fe may be another promising source indicator. For most of this paper, we will assume for simplicity that all Fe and Zn are in their divalent states, because Fe^{2+} is by far the dominant valence state in the mantle ($Fe^{3+}/Fe_T < 0.01$ in the upper mantle and ~ 0.1 in primitive MORB; Canil and O' Neill, 1996; Bezos and Humler, 2005) and, except for unusually reducing environments, Zn is always divalent. We will discuss the issue of Fe^{3+} at the end of the paper. Importantly, Fe^{2+} and Zn^{2+} have similar ionic radii in 6-fold coordination cation sites (0.78 and 0.74 Å, respectively; Mn^{2+} is 0.84 Å), which is how these elements are coordinated in olivine and orthopyroxene. Using a case study of Zn, Fe and Mn systematics in mafic and ultramafic systems, we show that $K_{D(Ol/melt)}^{Zn/Fe}$ and $K_{D(Opx/melt)}^{Zn/Fe}$ are close to 1, but much lower for clinopyroxene and garnet, in both peridotite and pyroxenite. This suggests that Zn/Fe is minimally fractionated during partial melting of peridotite mantle but strongly fractionated during melting of pyroxene or garnet-rich lithologies. We then examine the Zn/Fe systematics of oceanic basalts as a new tool for assessing source heterogeneities.

2. SAMPLES AND METHODS

The sampling consists of 57 mantle xenoliths that include 32 spinel or garnet peridotites from the Archean Tanzania craton and 25 spinel or garnet peridotites from western USA. Those from western USA include samples from Phanerozoic arc and extensional environments as well as Proterozoic lithospheric mantle. The equilibration temperatures of these xenoliths range from 800 to 1300 °C (based on garnet–pyroxene and two-pyroxene thermome-

ters) and thus they represent a broad spectrum of tectonic and thermal environments (Lee et al., 2001). The major element systematics of these xenoliths fall between fertile lherzolite compositions (pyrolite-like) and melt-depleted lithologies, such as harzburgites. Their major element systematics can be explained by variable degrees of melt depletion, with possible superimposed effects of refertilization. Our focus here on "canonical" peridotites is primarily to establish a baseline for mantle melting. We did not include lithologies, such as wehrlites, pyroxenites, olivine pyroxenites, websterites or Fe-rich dunites because such lithologies are likely cumulates, crystallized melts, or the products of extensive melt–rock reaction. Such lithologies are obvious candidates for major element heterogeneities in the mantle.

Whole-rock analyses on Tanzanian peridotites are reported in Lee (2001) and Lee and Rudnick (1999) and represent X-ray fluorescence measurements done at the University of Massachusetts, Amherst (details described in the references). Whole-rock chemistry of western USA samples were done at Rice University by solution inductively coupled plasma-mass spectrometry; results and techniques are published in Lee (2005). To assess data quality, BHVO-1 standard is reported in Table 1 along with the whole-rocks measurements performed at Rice University (Lee, 2005). BHVO-1 data are within error of recommended values, and typical uncertainties on Zn and Mn measurements are ∼5–10%.

In-situ mineral analyses were obtained by laser ablation inductively coupled plasma-mass spectrometer (LA-ICP-MS) at Rice University using a ThermoFinnigan Element II Sector ICP-MS coupled with a New Wave 213 nm laser ablation system. Ablation was performed on ∼150 μm thick sections under a pure He atmosphere. Typical spot sizes were 55 μm for external standards, 80 μm for clinopyroxenes and garnets, and 100 μm for orthopyroxenes and olivines. The energy density ranged between 15 and 20 J/cm² and the repetition rate was set at 10 Hz. Sensitivity was typically estimated at about 400,000 cps/ppm for La on a BHVO2 glass standard for a 55 μm, 10 Hz spot (15.6 ppm of La; Gao et al., 2002). Analyses were carried out in medium mass-resolution mode ($m/\Delta m = 3000$) since Fe suffers from major isobaric interferences from ArO^+. Analyses typically consisted of 12–15 measurements on gas background and ∼35 measurements during ablation of the sample. Drift associated with ablation yield or matrix effects were controlled by internal normalization (Longerich et al., 1996) using ^{30}Si (Si contents were determined from electron microprobe measurements or by normalizing all major element oxides to 100%). Background-corrected and internal standard-normalized signals were integrated and converted to concentrations using the in-house data reduction software. The external reproducibility and accuracy of the measurements were checked using USGS standards BHVO2-G, BCR2-G and BIR1-G (Gao et al., 2002). For each analysis, the detection limit was estimated at three times the standard deviation of the background divided by the sensitivity. Additional details of analytical procedures are given in Lee et al. (2008).

3. RESULTS

3.1. Zn, Mn and Fe in whole-rock peridotites and mantle minerals

Whole-rock ICP-MS and XRF analyses of major and trace elements in 57 peridotite xenoliths are reported in Table 1. Variations of Zn, Fe and Mn (ppm by weight) in selected mantle xenoliths are presented in Fig. 1 as a function of Mg# and Al_2O_3 wt%, which we use as melt depletion indices. Mg# increases and Al_2O_3 decreases in peridotite residues with increasing melt depletion (e.g. Walter, 2003). As shown in Fig. 1, Zn, Mn and Fe in peridotites show a slight negative correlation with Mg#. Zn and Fe show no variation with Al_2O_3 but Mn correlates slightly with Al_2O_3. Zn/Fe, Zn/Mn and Fe/Mn ratios in whole-rock peridotite xenoliths are plotted against Mg# and Al_2O_3 in Fig. 2, where it can be seen that these ratios are relatively constant with Mg# and Al_2O_3 (relative one sigma scatter for Zn/Fe is 10.5%, Zn/Mn is 13%, and Fe/Mn is 9%). As whole-rock Zn/Fe, Zn/Mn, and Fe/Mn ratios appear not to be significantly fractionated in peridotite residues during melting. The peridotite data define Zn/Fe ($\times 10^4$), Zn/Mn and Fe/Mn ratios of the mantle to be 8.5 (± 0.9), 0.05 (± 0.006) and 61 (± 5), respectively. We take these values as being representative of the upper mantle (Table 1). We note that these values are identical to within error to previous estimates of the primitive mantle compositions from McDonough and Sun (1995), Palme and O'Neill (2003) and Lyubetskaya and Korenaga (2007). We note that Zn and Mn measurements in the literature database may not be high-precision data or may contain systematic biases. This can probably explain the greater scatter of the literature data compared to our data, especially for Zn. However, motivated by the necessity to simultaneously examine Zn, Fe and Mn on the same rocks, we used the global literature database.

We now turn to Zn, Fe, and Mn systematics of mineral phases. In-situ LA-ICP-MS analyses on minerals in 24 peridotite xenoliths from western USA are shown in Table 2. For each sample, we analyzed at least five grains of the same phase to get representative concentrations. In a given sample, olivine contains the highest proportion of Zn (∼60 ppm) and Fe (∼80,000 ppm; FeO ∼10 wt%) while garnet is the most enriched in Mn (∼2300 ppm; MnO ∼0.3 wt%). Orthopyroxene is intermediate and clinopyroxene is the most depleted in Zn (∼13 ppm), Fe (∼23,000 ppm; FeO ∼3 wt%) and Mn (∼750 ppm; MnO ∼0.1 wt%).Zn/Fe ($\times 10^4$), Zn/Mn and Fe/Mn ratios obtained in olivine, clinopyroxene, orthopyroxene and garnet are plotted against each other in Fig. 3a–c, respectively. In such plots, each point essentially represents an individual, subsolidus exchange coefficient $K_{D(i/j)}^{A/B}$ between two mineral phases (Eq. (1)). Inter-mineral partition coefficients are reported in Table 3. If this quantity is a constant, then all the data for a given mineral pair should lie on an array that projects through the origin, the slope of this array being equivalent to the K_D. Regression lines through these data and forced through zero are thus presented. In most cases, the data arrays can be reasonably fit by regression

Table 1

Al_2O_3 wt%, Zn ppm, Mn and Fe ppm whole-rock compositions of BHVO-1 standard and peridotite xenoliths from western USA and northern Tanzania obtained by ICP-MS (Lee, 2001, 2005). Zn ppm in Tanzanian xenoliths was been obtained by XRF.

Sample	Standard	Western ISA xenoliths														
	BHVO-I	BC77	1026V	P7	P10	BC98-2	OK98-3	OK98-9	OK98-4	Ki5-1	Ki5-8	Ki5-16	Ki5-31	Ki5-32	Ki5-45	Ki5-110
Al_2O_3 wt%	13.80	2.29	2.96	2.98	1.67	2.63	2.79	3.27	3.62	1.65	4.13	0.58	2.14	2.19	1.53	0.94
Zn ppm	105.0	49.6	50.2	44.4	51.2	48.6	42.9	45.7	50.0	53.4	52.8	51.1	56.8	57.5	54.1	48.6
Mn ppm	1317	1075	1095	1033	1580	974	975	971	976	996	1015	899	1051	1115	1195	934
Fe ppm	85,537	60,280	54,520	64,150	61,750	57,610	60,500	60,690	60,250	65,940	63,010	62,850	64,080	69,930	71,890	65,060
$(Zn/Fe) * 10^4$	12.28	8.23	9.21	6.92	8.29	8.44	7.08	7.52	8.30	8.10	8.37	8.13	8.86	8.23	7.53	7.47
Zn/Mn	0.08	0.05	0.05	0.04	0.03	0.05	0.04	0.05	0.05	0.05	0.05	0.06	0.05	0.05	0.05	0.05
Fe/Mn	64.9	56.2	49.8	62.1	39.1	59.2	62.1	62.5	61.7	66.2	62.1	69.9	61.0	62.7	60.1	69.6

Sample	CiP98-8	CiP98-19	CiP98-62	CiP98-66	CP120	PM07	CP104	CP713	CP105	CP126
Al_2O_3 wt%	1.86	1.15	1.88	3.07	0.80	0.51	0.73	1.90	1.37	0.61
Zn ppm	49.7	58.4	53.8	65.0	40.3	49.0	50.5	46.2	51.7	44.6
Mn ppm	985	994	961	1271	848	838	688	862	862	798
Fe ppm	61,760	65,670	62,910	79,930	53,800	57,260	56,410	57,110	52,930	55,240
$(Zn/Fe) * 10^4$	8.05	8.89	8.55	8.14	7.49	8.56	8.95	8.09	9.78	8.07
Zn/Mn	0.05	0.06	0.06	0.05	0.05	0.06	0.07	0.05	0.06	0.06
Fe/Mn	62.7	66.1	65.4	62.9	63.4	68.4	82.0	66.3	61.4	69.2

Sample	Tanzania xenoliths															
	LB2	LB4	LB12	LB24	LB34	LB45	LB50-1	LB53	LBI	LB6	LB7	LB8	LB9	LB11	LB14	LB16	LB17
Al_2O_3 wt%	1.18	1.54	1.98	1.21	0.68	3.89	1.37	1.73	0.40	0.65	0.55	0.34	0.36	0.84	0.33	0.60	0.56
Zn ppm	46.0	47.5	59.0	49.0	77.0	60.0	55.0	58.0	48.0	49.0	58.0	44.0	45.0	51.0	51.0	55.0	58.0
Mn ppm	976	1011	1139	960	1084	1193	1069	1092	930	999	1022	875	891	999	945	991	1077
Fe ppm	51,240	58,560	64,870	53,790	72,200	64,830	60,590	61,670	49,570	57,380	58,340	49,780	50,550	55,860	55,600	56,100	57,590
$(Zn/Fe) * 10^4$	8.98	8.11	9.10	9.11	10.67	9.26	9.08	9.40	9.68	8.54	9.94	8.84	8.90	9.13	9.17	9.80	10.1
Zn/Mn	0.05	0.05	0.05	0.05	0.07	0.05	0.05	0.05	0.05	0.05	0.06	0.05	0.05	0.05	0.05	0.06	0.05
Fe/Mn	52.5	57.9	57.0	56.0	66.6	54.3	56.7	56.5	53.3	57.4	57.1	56.9	56.7	55.9	58.8	56.6	53.5
MgO wt%	45.9	43.5	42.1	45.7	45.8	38.7	44.2	43.9	47.3	47.7	48.0	17.4	47.5	46.4	48.9	46.3	44.8
Mg# (*100)	92.6	91.2	90.0	92.2	89.8	89.2	91.0	90.8	93.0	92.0	91.9	93.0	92.9	92.0	92.4	92.0	91.5

| Sample	LB18	LB19R	LB21	LB22	LB23	LB26	LB29	LB31	LB33	LB36	LB39	LB55	LB61	KAT1	LB58
Al_2O_3 wt%	0.42	0.82	0.30	0.67	0.54	0.45	0.88	1.02	0.60	0.88	0.86	0.76	0.50	0.66	0.52
Zn ppm	68.0	56.0	49.0	56.0	51.0	55.0	51.0	49.0	50.0	46.0	55.0	48.0	49.0	42.0	71.0
Mn ppm	1015	1123	914	1015	991	1038	968	1046	991	1007	1100	991	1015	852	1394
Fe ppm	64,600	66,180	50,690	57,850	56,170	55,000	55,240	56,780	56,860	54,020	60,130	52,780	54,400	55,440	81,680
$(Zn/Fe) * 10^4$	10.5	8.5	9.7	9.7	9.1	10.0	9.2	8.6	8.8	8.5	9.1	9.1	9.0	7.6	8.7
Zn/Mn	0.07	0.05	0.05	0.06	0.05	0.05	0.05	0.05	0.05	0.05	0.05	0.05	0.05	0.05	0.05
Fc/Mn	63.7	58.9	55.5	57.0	56.7	53.0	57.1	54.3	57.3	53.6	54.7	53.2	53.6	65.1	58.6
MgO wt%	47.1	45.8	48.8	45.9	47.3	47.0	46.5	45.3	46.5	45.4	44.0	46.1	47.7	46.6	45.1
Mg# (*100)	91.0	90.6	93.0	91.7	92.1	92.2	92.1	91.7	91.9	92.1	91.0	92.4	92.4	92.1	88.4
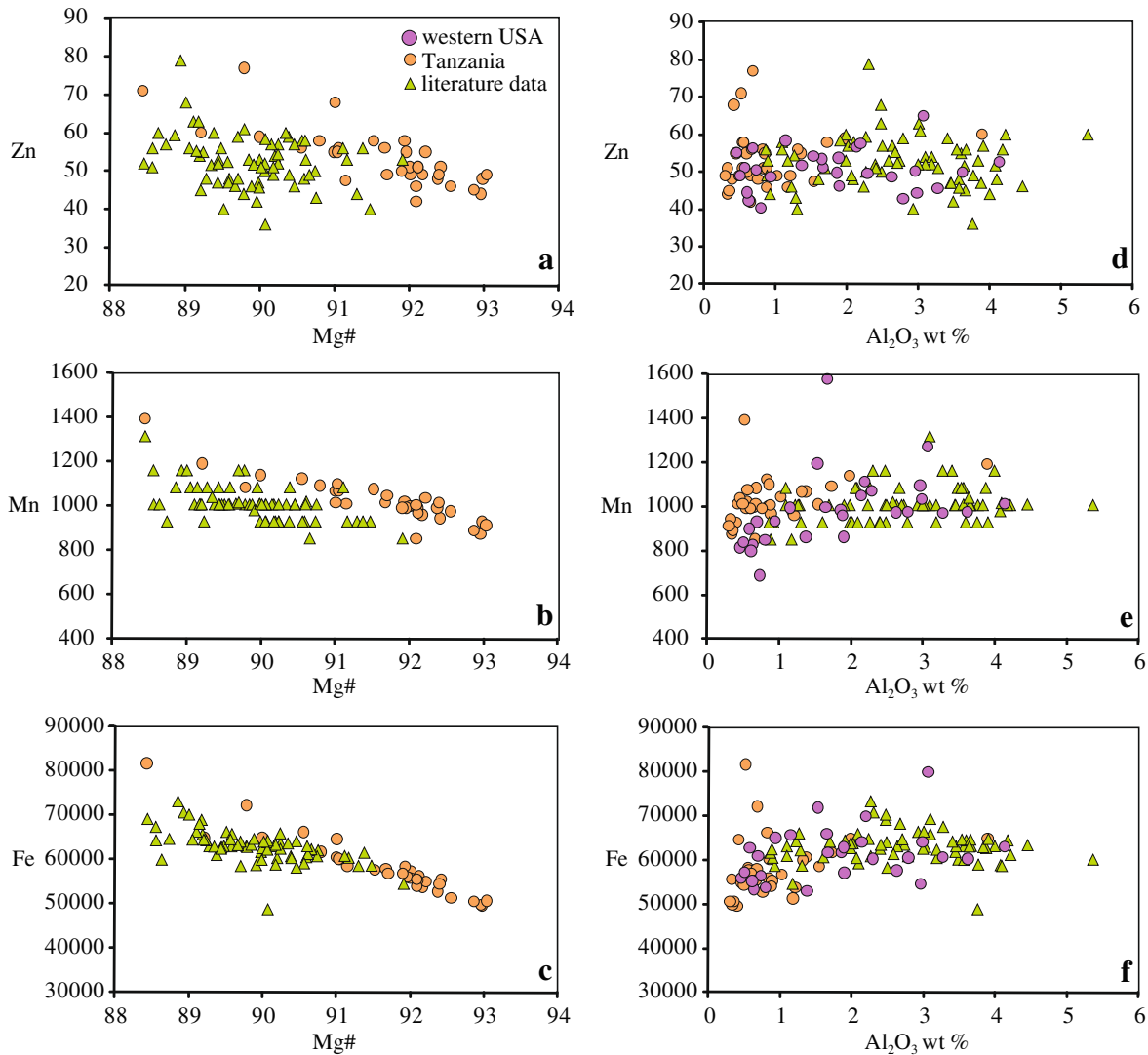
Fig. 1. (a–c) Zn, Mn and Fe ppm contents, respectively, vs. Mg# in peridotite xenoliths from northern Tanzania (Lee and Rudnick, 1999; Lee, 2001), along with literature data (Jagoutz et al., 1979; Menzies et al., 1987; Embeyisztin et al., 1989; Qi et al., 1995; Vaselli et al., 1995). (d–f) Zn, Mn and Fe ppm contents, respectively, vs. Al_2O_3 wt% in the samples named previously and in western USA peridotite xenoliths. Errors on measurements are smaller than the symbols.

lines forced through zero, indicating that apparent K_Ds are constant to within the precision of our data. Only Fe/Mn in garnet does not fit the regression, either because we lack systematic data on garnets or because the K_D cannot be considered as constant over the reequilibration conditions of the samples. Knowing that these xenoliths equilibrated over a wide spectrum of temperatures (800–1300 °C), the global constancy of K_Ds suggests that any temperature influence is relatively small compared to the resolution of the data. This feature is important as it justifies our later assumption that these inter-mineral partition coefficients most likely hold at solidus temperatures (1300–1400 °C).

Another key feature is shown in Fig. 3a. Zn/Fe in co-existing olivine and orthopyroxene are very similar ($Zn/Fe_{Opx} \sim Zn/Fe_{Ol}$), hence $K_{D(Opx/Ol)}^{Zn/Fe} \sim 1$, regardless of the absolute Zn/Fe or Zn and Fe content of the minerals or the host whole-rock. Additionally, olivine is the primary host

of Zn in peridotite. Based on our measurements and typical mineral modes of peridotites, olivine and orthopyroxene account for >95% of the total Zn budget in peridotites. This indicates that the whole-rock Zn/Fe of peridotites is strongly controlled by these two phases. In contrast, Zn/Fe is always lower in clinopyroxene and garnet compared to co-existing olivines, hence $K_{D(Cpx/Ol)}^{Zn/Fe}$ and $K_{D(Gt/Ol)}^{Zn/Fe}$ are <1. As for Zn/Mn and Fe/Mn, olivine displays the highest Zn/Mn and Fe/Mn ratios while co-existing orthopyroxene, clinopyroxene and garnet show low Zn/Mn and Fe/Mn ratios, hence $K_{D(Cpx/Ol)}$, $K_{D(Gt/Ol)}$, as well as $K_{D(Opx/Ol)}$ are all <1 for Zn/Mn and Fe/Mn (Fig. 3b and c).

3.2. Zn, Mn and Fe in oceanic basalts

We present here a literature compilation of whole-rock data from mid-ocean ridge basalts (MORB) and ocean is-
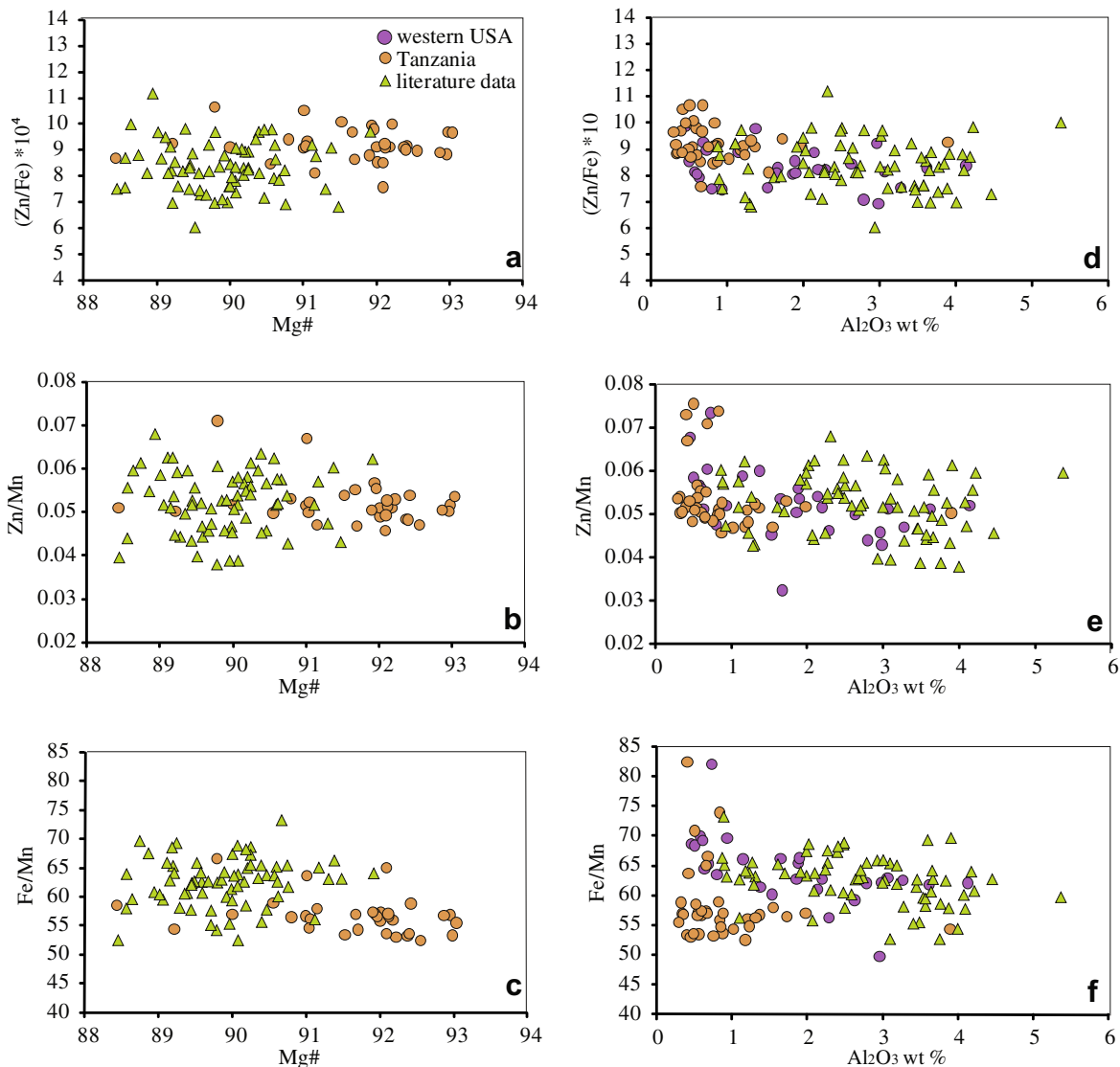
Fig. 2. (a–c) Zn/Fe ($\times 10^4$), Zn/Mn and Fe/Mn ratios, respectively, vs. Mg# in peridotite xenoliths from northern Tanzania (Lee and Rudnick, 1999; Lee, 2001), along with literature data (Jagoutz et al., 1979; Menzies et al., 1987; Embeyisztin et al., 1989; Qi et al., 1995; Vaselli et al., 1995). (d–f) Zn/Fe, Zn/Mn and Fe/Mn ratios, respectively, vs. Al$_2$O$_3$ wt% in the samples named previously and in western USA peridotite xenoliths. Errors on measurements are smaller than the symbols.

land basalts (OIB) sampled over different locations worldwide. The entire database is published and available from the GEOROC database: http://georoc.mpch-mainz.gwdg.de/georoc/. We are aware that the precision and accuracy of the literature data are not as good as in Humayun et al. (2004) and Qin and Humayun (2008), where a concerted effort was taken to generate high-precision Fe/Mn data. However, Zn data are not presented in these studies. Thus, motivated by the necessity to simultaneously examine Zn, Fe and Mn on the same rocks, we were constrained to use the global literature database.

Primary magmas, i.e., magmas that have not experienced fractional crystallization, are the ideal samples for our study but primary magmas are rare. We thus focus on the most primitive oceanic basalts (>8.5 wt% MgO) because these basalts are likely to have the simplest crystalli-

zation histories. For instance, in many cases, olivine crystallization dominates the early differentiation of such basalts, hence the composition of the primary parental magma can be reasonably inferred if the behavior of Zn, Mn and Fe in olivine during fractionation is well-understood. More evolved magmas suffer from cotectic crystallization, making it difficult to arrive at unique correction procedures for fractionation. We have also avoided basalts with unusually high MgO contents (>17–18 MgO wt%) as such rocks may have accumulated olivine (e.g. picrites) and are thus not true melt compositions; these basalts will not be discussed further.

Evolved magmas with MgO < 8.5 wt% show clear correlations between the abundances and relative proportions of Zn, Mn and Fe versus MgO, underscoring the fact that Zn, Mn and Fe systematics in evolved basalts do not preserve

Table 2
Zn ppm, Mn ppm and Fe ppm compositions of olivine (Ol), orthopyroxene (Opx), clinopyroxene (Cpx) and garnet (Gt) in western USA peridotite xenoliths.

Sample		OK98-2	OK98-3	OK98-4	OK98-9	P6	P7	BC98-2	BC77	1026V	SC99-2	CLB47	CLB22	CLB53
Zn ppm	Ol	52.5	48.8	54.1	46.1	63.6	27.2	58.9	45.7	47.3	49.7	60.1	52.7	60.1
	Opx	39.7	29.0	38.9	37.5	40.5	21.5	33.5	33.6	31.8	34.2	40.3	38.3	40.8
	Cpx	10.63	8.36	8.87	8.95	6.69	10.45	6.09	7.24	6.18	9.51	10.62	10.11	11.84
	Gt								7.24	7.10				
Mn ppm	Ol	900	1230	1059	1199	948	1071	1304	820	774	1497	1303	1218	1317
	Opx	1160	1314	1061	1314	1037	1097	1095	1016	1106	1166	1310	1152	1177
	Cpx	623	715	656	766	509	628	541	672	648	828	743	685	818
	Gt								2859	4193				
Fe ppm	Ol	66,940	81,530	72,870	80,230	93,790	88,020	86,960	76,860	81,520	91,010	79,990	67,760	82,840
	Opx	52,020	58,360	50,230	62,210	51,730	53,840	50,410	44,680	60,240	49,400	51,910	46,400	48,860
	Cpx	23,980	28,880	23,790	30,290	17,690	17,700	14,480	19,110	19,810	24,120	25,160	16,750	27,010
	Gt								66515	83208				
Zn/Fe (*10^4)	01	7.84	5.99	7.42	5.75	6.78	3.09	6.77	5.94	5.81	5.46	7.52	7.77	7.25
	Opx	7.64	4.98	7.75	6.03	7.83	3.99	6.64	7.53	5.28	6.93	7.76	8.25	8.36
	Cpx	4.43	2.89	3.73	2.95	3.79	0.00	4.21	3.79	3.12	3.94	4.22	6.04	4.38
	Gt								1.09	0.853				
Zn/Mn	Ol	0.058	0 040	0.051	0.038	0.067	0.025	0.045	0.056	0.061	0.033	0.046	0.043	0.046
	Opx	0.034	0.022	0.037	0.029	0.039	0.020	0.031	0.033	0.029	0.029	0.031	0.033	0.035
	Cpx	0.017	0.012	0.014	0.012	0.013	0.017	0.011	0.011	0.010	0.011	0.014	0.015	0.014
	Gt								0.003	0.002				
Fe/Mn	01	74.4	66.3	68.8	66.9	98.9	82.2	66.7	93.7	105	60.8	61.4	55.6	62.9
	Opx	44.8	44.4	47.3	47.3	49.9	49.1	46.0	44.0	54.5	42.4	39.6	40.3	41.5
	Cpx	38.5	40.4	36.3	39.6	34.7	28.2	26.8	28.4	30.6	29.1	33.9	24.5	33.0
	Gt								23.3	19.8				

| Sample		CLB55	CLB58	CLB21	CLB43	CLB50	C1.B71	TH1	TH2	TH3	TH4	SC991
Zn ppm	Ol	64.1	53.0		59.1	52.4	80.0	63.2	58.3	75.5	60.7	51.9
	Opx	35.5	35.5	37.8	32.7	37.4	46.3	34.9	36.8		35.0	34.1
	Cpx	13.4	9.85	10.4	7.70		11.2	13.1		16.3		10.4
	Gt									13.9		
Mn ppm	Ol	1485	1357		1273	1237	1397	961	1019	1001	1057	1192
	Opx	1190	982	1253	1102	1055	1121	1015			989	1085
	Cpx	756	842	745	665		710	749		854		818
	Gt									2227		
Fe ppm	Ol		67,530		73,850	76,030	81,370	69,040	70,650	86,260	78,610	88,270
	Opx	53,140	38,400	53,670	40,970	46,940	48,580	40,570	40,620		45,170	49,920
	Cpx	22,850	19,450	20,460	18,980		22,530	19,470		28,030		24,540
	Gt									60,440		
Zn/Fe (*10^4)	Ol	7.84	7.85		8.00	6.89	9.84	9.16	8.25	8.75	7.72	5.87
	Opx	6.67	9.26	7.04	7.98	7.97	9.52	8.59	9.06		7.75	6.84
	Cpx	5.86	5.06	5.06	4.05		4.96	6.68		5.84		4.23
	Gt									2.30		
Zn/Mn	Ol	0.043	0.039		0.046	0.042	0.057	0.066	0.057	0.075	0.057	0.043
	Opx	0.030	0.036	0.030	0.030	0.035	0.041	0.034	0.037		0.035	0.031
	Cpx	0.018	0.012	0.014	0.012		0.016	0.018		0.019		0.013
	Gt									0.006		
Fe/Mn	Ol	55.1	49.8		58.0	61.5	58.3	71.9	69.4	86.2	74.4	74.1
	Opx	44.7	39.1	42.8	37.2	44.5	43.3	40.0	40.9		45.7	46.0
	Cpx	30.2	23.1	57.5	28.6		31.7	26.0		32.8		30.0
	Gt									27.1		
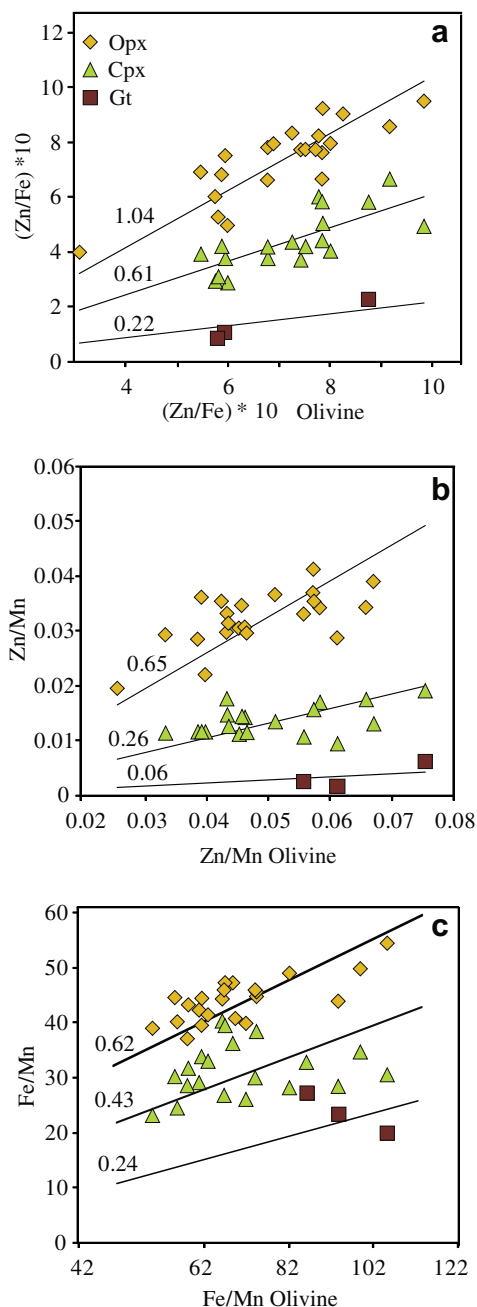
Fig. 3. (a–c) Zn/Fe ($\times 10^4$), Zn/Mn and Fe/Mn ratios, respectively, in orthopyroxene (Opx), clinopyroxene (Cpx) and garnet (Gt) vs. Zn/Fe ($\times 10^4$), Zn/Mn and Fe/Mn, respectively, in olivine (Ol). Minerals measurements have been performed in western USA peridotite xenoliths. Inter-mineral exchange coefficients ($K_{D(\text{phase/olivine})}^{\text{ratio}}$) are indicated on the regression line and corresponds to the slope of the linear regression line (black line).

Table 3
Inter-mineral exchange coefficients measured in co-existing olivine, orthopyroxene, clinopyroxene and garnet from peridotite xenoliths from western USA and bulk exchange coefficients calculated from three independent approaches (see Section 4.2).

Inter-mineral exchange partition coefficients

$K_{D(\text{Opx/Ol})}^{\text{Zn/Fe}}$	1.04	$K_{D(\text{Opx/Ol})}^{\text{Zn/Mn}}$	0.65	$K_{D(\text{Opx/Ol})}^{\text{Fe/Mn}}$	0.62
$K_{D(\text{Cpx/Ol})}^{\text{Zn/Fe}}$	0.61	$K_{D(\text{Cpx/Ol})}^{\text{Zn/Mn}}$	0.26	$K_{D(\text{Cpx/Ol})}^{\text{Fe/Mn}}$	0.43
$K_{D(\text{Gt/Ol})}^{\text{Zn/Fe}}$	0.22	$K_{D(\text{Gt/Ol})}^{\text{Zn/Mn}}$	0.06	$K_{D(\text{Gt/Ol})}^{\text{Fe/Mn}}$	0.24

	Approach 1	Approach 2	Approach 3
Bulk exchange partition coefficients			
$K_{D(\text{perid/melt})}^{\text{Zn/Fe}}$	0.85–0.92	0.94–1	0.85–0.9
$K_{D(\text{perid/melt})}^{\text{Zn/Mn}}$	1	0.72–0.8	0.89
$K_{D(\text{perid/melt})}^{\text{Fe/Mn}}$	1.1	0.76–0.8	1.1

individual magma suites (e.g. MORB and the different ocean islands) display very narrow variations with MgO content (Fig. 5d–f), indicating that the global spread in data is not related to analytical issues. Instead, the constancy of individual magmatic suites for MgO > 8.5 wt% indicates that early crystal fractionation, presumably dominated by olivine, does not significantly modify these ratios. Individual OIB suites are thus characterized by constant Zn/Fe, Zn/Mn and Fe/Mn ratios that appear to preserve primary magmatic signatures. Although the majority of MORB are too evolved to preserve primary signatures, the most primitive MORB show relatively constant Zn/Fe, Zn/Mn and Fe/Mn ratios as a function of MgO. We take these primitive MORB samples, rather than the average of all MORB, as representative of the Zn–Fe–Mn ratios of the parental MORB magma.

Taking the Zn/Fe, Zn/Mn and Fe/Mn ratios of primitive MORB and OIB, the following observations can be made. Primitive MORB are almost identical to the mantle field as constrained by the peridotite xenoliths discussed above. Primitive OIB have Zn/Fe, Zn/Mn and Fe/Mn ratios ranging from values similar to those of primitive MORB to values significantly higher. For example, OIB suites from the Society Islands, Cape Verde and the Samoan Islands have much higher Zn/Fe ratios than primitive MORB and the mantle. In contrast, OIB suites like the Galapagos Islands and Iceland, which are near or on active ridges, have Zn/Fe ratios similar to those of primitive MORB. The meaning of these differences will be discussed in the next section.

4. DISCUSSION

4.1. Inter-mineral exchange coefficients

In Section 3, we estimated Zn/Fe, Zn/Mn and Fe/Mn inter-mineral exchange coefficients between olivine, orthopyroxene, clinopyroxene and garnet in peridotite xenoliths from western USA (Table 3) and showed that they are constant over a wide range of equilibration temperatures as evi-

primary magma signatures (Fig. 4). In contrast, Zn, Mn and Fe contents as well as their ratios do not vary significantly with MgO in OIB and MORB that have MgO > 8.5 wt% (Figs. 4 and 5). It is possible that this apparent constancy with MgO is simply due to the large degree of scatter associated with the global OIB or MORB datasets. However, Zn/Fe, Zn/Mn and Fe/Mn ratios of
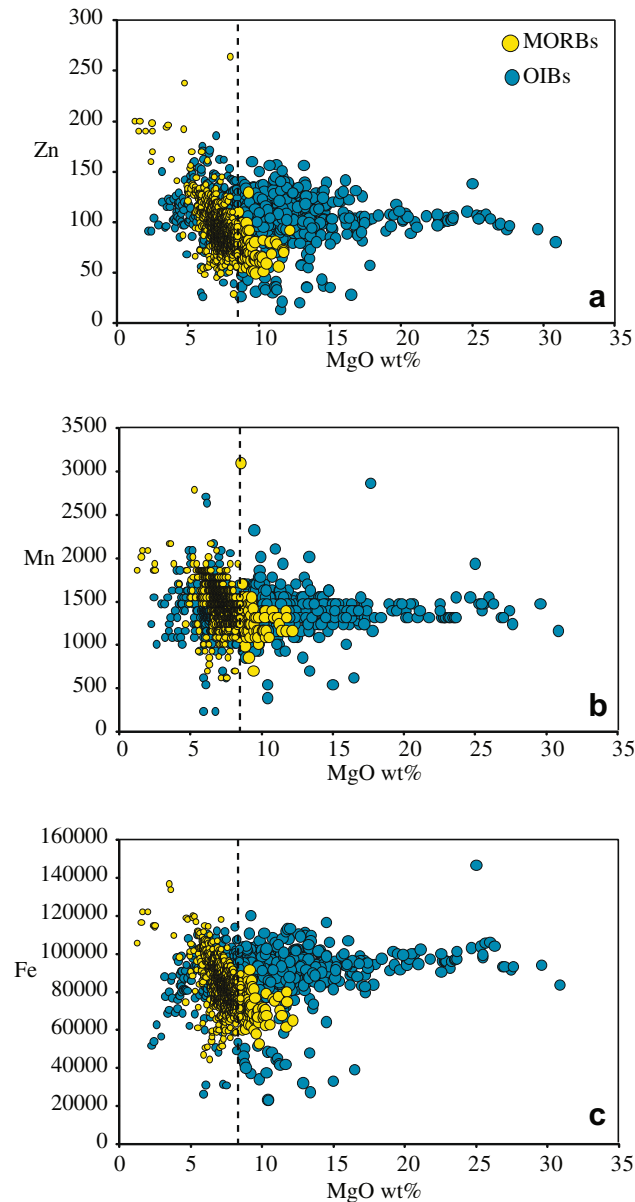
Fig. 4. (a–c) Zn, Mn and Fe ppm contents, respectively, vs. MgO wt% in MORB and OIB. Smaller symbols to the left represent the most evolved oceanic basalts that contain less than 8.5 wt% MgO (indicated by the dashed line). These basalts may have experienced fractionation of several phases before eruption.

denced by the fact that elemental ratios between minerals from many different samples can be fit by a regression line that intersects the origin. This suggests that the inter-mineral K_Ds of these ratios are insensitive to temperature (to within error of our measurements) in the 800–1300 °C temperature range (equilibration temperatures of our xenoliths), and based on this observation, we assume these K_Ds are also valid at solidus temperatures.

Significant differences arise in the partitioning of Zn/Fe, Zn/Mn and Fe/Mn between olivine and orthopyroxene, and between olivine and clinopyroxene and garnet. For example, as shown above, Zn/Fe ratios are equally fractionated between olivine, orthopyroxene and melt, but strongly

fractionated when garnet and clinopyroxene are considered. These differences can probably be explained by the crystal structure where these metal transition ions are hosted. Zn^{2+}, Mn^{2+} and Fe^{2+} all have ionic radii comparable to Mg^{2+} in 6-fold coordination. In olivine and orthopyroxene, all of the metal cation sites are in 6-fold coordination, which probably explains why first series transition metals partition in a similar way between these two minerals. However, in clinopyroxene, the M2 site is probably in 8-fold coordination and the M1 site is in 6-fold coordination. In garnet, divalent cations occupy the large 8-fold coordination site (Meagher, 1982). Because the radii of these divalent cations in 8-fold coordination differ from those in
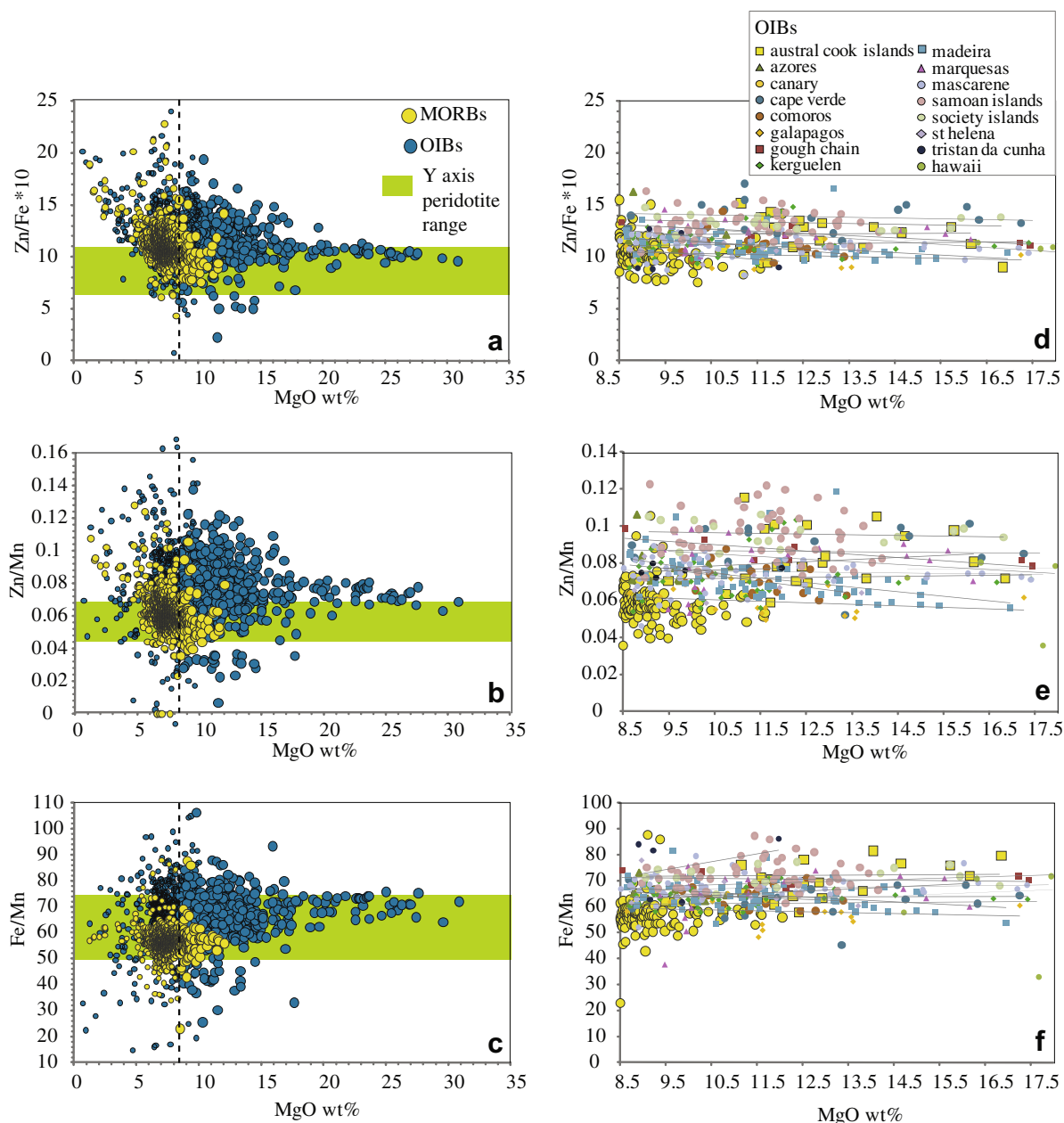
Fig. 5. (a–c) Zn/Fe ($\times 10^4$), Zn/Mn and Fe/Mn ratios vs. MgO wt% in MORB and OIB. Smaller symbols to the left represent the most evolved oceanic basalts that contain less than 8.5 wt% MgO (indicated by the dashed line). These basalts may have experienced fractionation of several phases before eruption. (d–f) Zn/Fe ($\times 10^4$), Zn/Mn and Fe/Mn ratios respectively vs. MgO wt% in MORB and individual OIB suites that contain more than 8.5 wt% MgO and less than 17.5 wt% MgO. This corresponds approximately to the olivine fractionation window. The black lines correspond to the regression lines of individual OIB suites.

6-fold coordination, partitioning of Zn, Mn and Fe in clinopyroxene and garnet are expected to differ significantly from olivine and orthopyroxene.

In the following discussion we will use the inter-mineral exchange coefficients derived in Section 3 to obtain bulk peridotite–melt exchange coefficients. We point out that we have not accounted for spinel in this study. However, its abundance is very low in residual peridotites (<2%). Thus, even though spinels can have high Zn, Fe and Mn contents (Oreilly et al., 1991), we consider here that the proportional contribution of spinel to the Zn, Mn and Fe bud-

get of the whole-rock is negligible. This is confirmed by the fact that Zn, Fe and Mn contents are identical to within error in measured whole-rocks and in calculated whole-rock compositions reconstructed using Zn, Fe and Mn contents of all the mineral phases (except for spinel) along with their modal proportions.

4.2. Peridotite–melt exchange coefficients

The purpose of this section is to constrain the bulk exchange coefficients $K_{D(peridotite/melt)}$ for Zn/Fe and Zn/Mn be-

tween a melt and its solid residue. We focus our efforts primarily on Zn/Fe and Zn/Mn because Fe/Mn systematics have already been investigated by Humayun et al. (2004) and because there are relatively few constraints on Zn partitioning. Our analysis of peridotite minerals provides well-constrained inter-mineral exchange coefficients (Section 4.1) but we are missing the mineral/melt exchange coefficients. Here we estimate the bulk exchange coefficients of Zn/Fe, Zn/Mn and Fe/Mn using three independent approaches. In the first approach, we use experimentally determined olivine–melt partition coefficients $D_{\text{Ol/melt}}$ ($D_{\text{Ol/melt}}^A = A_{\text{Ol}}/A_{\text{melt}}$, where A is an element) and our inter-mineral exchange coefficients to get $K_{D(\text{peridotite/melt})}$. In the second approach, we use Zn, Mn and Fe concentrations from natural phenocryst–magma pair to calculate $K_{D(\text{Ol/melt})}$, which we then combine with inter-mineral $K_D s$ to get $K_{D(\text{peridotite/melt})}$. In the third approach, we estimate $K_{D(\text{peridotite/melt})}$ indirectly using MORB and peridotite data.

4.2.1. Approach 1

The objective of this approach is to obtain an olivine–melt exchange coefficient $K_{D(\text{Ol/melt})}^{\text{Zn/Fe}}$ from elemental partition coefficients $D_{\text{Ol/melt}}^{\text{Zn}}$ and $D_{\text{Ol/melt}}^{\text{Fe}}$ using the relationship $K_{D(\text{Ol/melt})}^{\text{Zn/Fe}} = D_{\text{Ol/melt}}^{\text{Zn}}/D_{\text{Ol/melt}}^{\text{Fe}}$. Although there are many Fe partitioning experiments, few Zn partitioning data are available. For Zn, we use the experiments of Ramsay et al. (1984) who showed that $D_{\text{Ol/melt}}^{\text{Zn}}$ depends on the MgO content of the melt, which itself is an indirect measure of temperature in basaltic magmas saturated with olivine (Roeder and Emslie, 1970). Bedard (2005) suggested the following equation to describe $D_{\text{Ol/melt}}^{\text{Zn}}$

$$\ln(D_{\text{Ol/melt}}^{\text{Zn}}) = -0.6740 \text{MgO} + 1.696 \quad (2)$$

where MgO is in wt% in the melt. With the aid of the LEPR database (http://lepr.ofm-research.org), we compiled ~300 published experiments where basaltic melt was in equilibrium with olivine and orthopyroxene between temperatures of 1220–1500 °C and pressures of 0.7–2.4 GPa. These experimental liquids are thus representative of primary mantle-derived liquids. Using the MgO content of the liquids, we calculate $D_{\text{Ol/melt}}^{\text{Zn}}$ using Eq. (2). We then use the FeO and MgO contents of the same liquids to calculate the FeO and MgO contents of co-existing olivines by assuming $K_{D(\text{Ol/melt})}^{\text{Fe/Mg}} = 0.3$ and olivine stoichiometry (Roeder and Emslie, 1970). This allows us to calculate $D_{\text{Ol/melt}}^{\text{Fe}}$ on the same experiments as we calculated $D_{\text{Ol/melt}}^{\text{Zn}}$. $K_{D(\text{Ol/melt})}^{\text{Zn/Fe}}$ is then calculated by dividing $D_{\text{Ol/melt}}^{\text{Zn}}$ by $D_{\text{Ol/melt}}^{\text{Fe}}$. Although $D_{\text{Ol/melt}}^{\text{Zn}}$ and $D_{\text{Ol/melt}}^{\text{Fe}}$ each depend on temperature, the exchange coefficient $K_{D(\text{Ol/melt})}^{\text{Zn/Fe}}$ does not depend significantly on temperature as the average $K_{D(\text{Ol/melt})}^{\text{Zn/Fe}}$ is 0.92 ± 0.07 (1σ). The lack of strong temperature dependence is also consistent with the constancy of inter-mineral exchange coefficients over a wide temperature range as discussed above. This is not surprising as it is well-known that $D_{\text{Ol/melt}}^{\text{Fe}}$ and $D_{\text{Ol/melt}}^{\text{Mg}}$ depend on temperature but their ratio $K_{D(\text{Ol/melt})}^{\text{Fe/Mg}}$ varies much less with temperature (Roeder and Emslie, 1970).

$K_{D(\text{peridotite/melt})}^{\text{Zn/Fe}}$ can be extrapolated from $K_{D(\text{Ol/melt})}^{\text{Zn/Fe}}$ using inter-mineral partition coefficients obtained in this study (Table 3) the mineral modes in the peridotite of interest, and the Fe contents of the minerals (Table 2) as follows

$$K_{D(\text{peridotite/melt})}^{\text{Zn/Fe}}$$
$$= K_{D(\text{Ol/melt})}^{\text{Zn/Fe}} \left[X_{\text{Ol}}^{\text{Fe}} + X_{\text{Opx}}^{\text{Fe}} K_{\text{Opx/Ol}}^{\text{Zn/Fe}} + X_{\text{Cpx}}^{\text{Fe}} K_{\text{Cpx/Ol}}^{\text{Zn/Fe}} + X_{\text{Gt}}^{\text{Fe}} K_{\text{Gt/Ol}}^{\text{Zn/Fe}} \right] \quad (3)$$

where $X_j^{\text{Fe}} = \sum C_j^{\text{Fe}} x_j / C_{\text{peridotite}}^{\text{Fe}}$ is the fraction of Fe in phase j relative to the whole-rock (and C_j and $C_{\text{peridotite}}$ represent the concentration of Fe in phase j and the bulk rock and x_j is the weight fraction of phase j in the rock). The last term in Eq. (3) corresponds to garnet, but it should be replaced with spinel if spinel lherzolite melting is considered, such as during MORB melting. Thus, assuming typical Fe contents in peridotitic minerals and a moderately depleted garnet peridotite (Ol = 61%; Opx = 33.2%; Cpx = 2.2%; Gt = 3.6%; Simon et al., 2003) we find $K_{D(\text{peridotite/melt})}^{\text{Zn/Fe}}$ to be 0.9. Fertile garnet peridotites (Ol = 63%; Opx = 17%; Cpx = 12%; Gt = 8%; Jeffcoate et al., 2007) would yield a $K_{D(\text{peridotite/melt})}^{\text{Zn/Fe}}$ of 0.85. Individual mineral/melt $K_D s$ calculated from a $K_{D(\text{Ol/melt})}^{\text{Zn/Fe}}$ of 0.92 are $K_{D(\text{Opx/melt})}^{\text{Zn/Fe}} = 0.96$, $K_{D(\text{Cpx/melt})}^{\text{Zn/Fe}} = 0.56$, and $K_{D(\text{Gt/melt})}^{\text{Zn/Fe}} = 0.20$. For comparison, we calculated $K_{D(\text{Opx/melt})}^{\text{Zn/Fe}}$ using the same approach as previously described in Bedard (2005) for $K_{D(\text{Ol/melt})}^{\text{Zn/Fe}}$. Bedard (2007) showed that:

$$\ln(D_{\text{Opx/melt}}^{\text{Zn}}) = -0.543531 \text{MgO} + 1.284692 \quad (4)$$

This yields $K_{D(\text{Opx/melt})}^{\text{Zn/Fe}} = 0.9 \pm 0.09 (1\sigma)$, which is consistent with our observation that olivine and orthopyroxene do not fractionate Zn/Fe. While we did not measure Zn/Fe ratios of spinels, the modal abundance of spinel is so small in spinel-facies peridotites that spinels account for a negligible amount of the total Zn and Fe budget in a peridotite. A similar calculation done for spinel peridotites (Ol = 78%; Opx = 17%; Cpx = 5%) yields a $K_{D(\text{peridotite/melt})}^{\text{Zn/Fe}}$ of ~0.92. As for Zn/Fe systematics, $K_{D(i/\text{melt})}^{\text{Fe/Mn}}$ can be taken directly from experimental data as Mn is often measured during electron microprobe analyses. The experiments of Walter (1998) provide an internally consistent dataset of peridotite residue-melt and mineral-melt exchange coefficients, $K_{D(\text{peridotite/melt})}^{\text{Fe/Mn}} \sim 1.1$, $K_{D(\text{Ol/melt})}^{\text{Fe/Mn}} \sim 1.3$, $K_{D(\text{Opx/melt})}^{\text{Fe/Mn}} \sim 0.85$, $K_{D(\text{Cpx/melt})}^{\text{Fe/Mn}} \sim 0.69$, and $K_{D(\text{Gt/melt})}^{\text{Fe/Mn}} \sim 0.6$. From $K_{D(\text{peridotite/melt})}^{\text{Fe/Mn}}$ and $K_{D(\text{peridotite/melt})}^{\text{Zn/Fe}}$, we get a Zn/Mn exchange coefficient $K_{D(\text{peridotite/melt})}^{\text{Zn/Mn}} \sim 1$. Thus, Approach 1 suggests that Zn, Fe, and Mn behave similarly during peridotite melting.

4.2.2. Approach 2

In our second approach, we calculate $K_{D(\text{Ol/melt})}^{\text{Zn/Fe}}$, $K_{D(\text{Ol/melt})}^{\text{Zn/Mn}}$ and $K_{D(\text{Ol/melt})}^{\text{Fe/Mn}}$ using published Zn, Mn and Fe contents in olivine phenocrysts and glasses in primitive Hawaiian basalts (see Norman et al., 2005; olivine B–lava 8 with $K_{D(\text{Ol/melt})}^{\text{Fe/Mg}} = 0.26$). According to these phenocryst–magma pairs, $K_{D(\text{Ol/melt})}^{\text{Zn/Fe}} = 1.02$, $K_{D(\text{Ol/melt})}^{\text{Zn/Mn}} = 1$ and $K_{D(\text{Ol/melt})}^{\text{Fe/Mn}} = 1$.

Then, using the inter-mineral partition coefficients obtained in this study, the same peridotite compositions in Section 4.2, and Eq. (3), we calculate that $K_{D(\text{peridotite/melt})}^{\text{Zn/Fe}} = 1$, $K_{D(\text{peridotite/melt})}^{\text{Zn/Mn}} = 0.8$ and $K_{D(\text{peridotite/melt})}^{\text{Fe/Mn}} = 0.8$ for a depleted garnet peridotite and $K_{D(\text{peridotite/melt})}^{\text{Zn/Fe}} = 0.94$, $K_{D(\text{peridotite/melt})}^{\text{Zn/Mn}} = 0.72$ and $K_{D(\text{peridotite/melt})}^{\text{Fe/Mn}} = 0.76$ for a fertile garnet peridotite. The Fe/Mn exchange coefficients are lower than those estimated from Walter's data in Section 4.2.1 because the phenocryst–magma-determined $K_{D(\text{Ol/melt})}^{\text{Fe/Mn}}$ of 1.0 is lower than that from Walter's experiments (1.3). It is also important to note that these are approximations from direct measurements of one natural sample and thus the exchange coefficients presented in this subsection could have large uncertainties.

4.2.3. Approach 3

We also estimate the exchange coefficients of Zn/Fe, Zn/Mn and Fe/Mn between peridotite and melt using their ratios in average peridotites over their ratios in primitive MORB. In this scheme, we assume that MORB sample a sufficiently large length scale in the mantle so that the MORB-source is representative of the average upper mantle which we assume to be canonical peridotite (Depleted MORB Mantle; Workman and Hart, 2005). We appreciate that the source of MORB probably contains components of recycled crust (Hirschmann and Stolper, 1996; Eiler et al., 2000). However, the overall composition of MORB requires that peridotite is by far the most dominant lithology in their mantle source region – Sobolev et al. (2007) suggested that DMM contains ~5% of recycled oceanic crust or that the average composition of the source integrated over >10 km lengthscales is peridotite (Workman and Hart, 2005). As shown above, Zn/Fe, Zn/Mn and Fe/Mn of peridotites are relatively constant (Fig. 2), implying that melt extraction does not fractionate these ratios significantly in the residue. We can thus take peridotite values of these ratios and divide by the same values in primitive MORB. Because Zn/Fe, Zn/Mn and Fe/Mn ratios of the most primitive MORB are remarkably similar to those of whole-rocks peridotites (Fig. 5), we obtain $K_{D(\text{peridotite/melt})}^{\text{Zn/Fe}}$ ~ 0.85–0.9, $K_{D(\text{peridotite/melt})}^{\text{Zn/Mn}}$ ~ 0.89, $K_{D(\text{peridotite/melt})}^{\text{Fe/Mn}}$ ~ 1.1. These results are relatively similar to what has been obtained from approach 1 and 2 for Zn/Fe and Zn/Mn. It is relatively higher for Fe/Mn than approach 2 but consistent with approach 1 and $K_{D(\text{Ol/melt})}^{\text{Fe/Mn}} = 1.05–1.11$ obtained by Humayun et al. (2004).

4.3. Sensitivity of the ratios to mineralogical variations

Estimations of the inter-mineral K_Ds on natural samples and of bulk peridotite K_Ds using three independent approaches give consistent results and show that Zn/Fe, Zn/Mn and Fe/Mn (1) are minimally fractionated during melting of typical residual peridotites and (2) relatively insensitive to olivine crystallization. However, these ratios are fractionated when clinopyroxene or garnet is the dominant crystallizing or residual phase. If clinopyroxene or garnet is the dominant residual phase, complementary liquids would

be characterized by anomalously high Zn/Fe, Zn/Mn and Fe/Mn ratios. These ratios in primitive basalts may thus be reliable proxies for detecting major element or lithological heterogeneities in the mantle that deviate from average peridotitic mantle.

There are, nevertheless, subtle differences in the applicability of these ratios in detecting heterogeneities. Major element heterogeneities could be 'soft' or extreme. We call 'soft' heterogeneities those which are within the peridotite field, that is, when the lithology is dominated by olivine and orthopyroxene but the ratio of olivine and orthopyroxene deviates from typical residual peridotites. For instance, dunite channels are likely to be an important part of oceanic lithospheric mantle (Kelemen et al., 1995) while orthopyroxene-enriched harzburgites are found in continental lithospheric mantle (Boyd, 1998). Such lithologies are usually thought to represent typical residual peridotites that have experienced melt–rock reaction (Kelemen et al., 1992). At the other extreme are heterogeneities that have such large modal abundances of pyroxenes (clinopyroxene and orthopyroxene) and/or garnet that they can no longer be classified as peridotites, but are better described as pyroxenites (websterites, clinopyroxenites, orthopyroxenites, eclogites) and wehrlites. Such lithologies, as briefly mentioned in the Introduction, represent crystallized basaltic liquids, cumulates or melt-peridotite reaction products.

Zn/Fe, Zn/Mn and Fe/Mn should all fractionate considerably during pyroxenite melting. However, Zn/Mn and Fe/Mn may be more affected than Zn/Fe due to heterogeneities within the peridotite field itself because the major phases (olivine and orthopyroxene) have inter-mineral exchange partition coefficients for Zn/Mn and Fe/Mn $\neq 1$. This could be problematic for deciphering whether variations in oceanic basalts are related to subtle variations in olivine/orthopyroxene ratios in peridotites or to the presence of fundamentally non-peridotitic lithologies in the mantle source, such as recycled oceanic crust. Indeed, Fe/Mn ratios in refractory peridotites exhibit more scatter than in fertile peridotites (Fig. 2f). Zn/Fe, on the other hand, is expected to remain unfractionated during melting of most peridotitic lithologies, independent of variations in the olivine/orthopyroxene ratio. Zn/Fe therefore is a powerful geochemical index for tracking the presence of clinopyroxene- and/or garnet-rich lithologies in the mantle source. For this reason, and because Fe/Mn systematics have already been extensively studied, we will focus on Zn/Fe ratios in the following discussion as a tool for tracking lithological heterogeneities that deviate from peridotite mantle.

4.4. What is in the source of oceanic basalts?

4.4.1. Peridotite source

Oceanic basalts have Zn/Fe ($\times 10^4$) ratios ranging from average upper mantle values (~8.5) up to values as high as 15–16. In Fig. 6, Zn/Fe ($\times 10^4$) ratios of MORB and individual OIB suites have been calculated from their regression lines (Fig. 5) for MgO wt% = 12 (Table 4). Error bars on Zn/Fe ratios of the melts correspond to the standard error of the predicted Zn/Fe-value for each MgO value in the regression. Our objective here is to assess whether
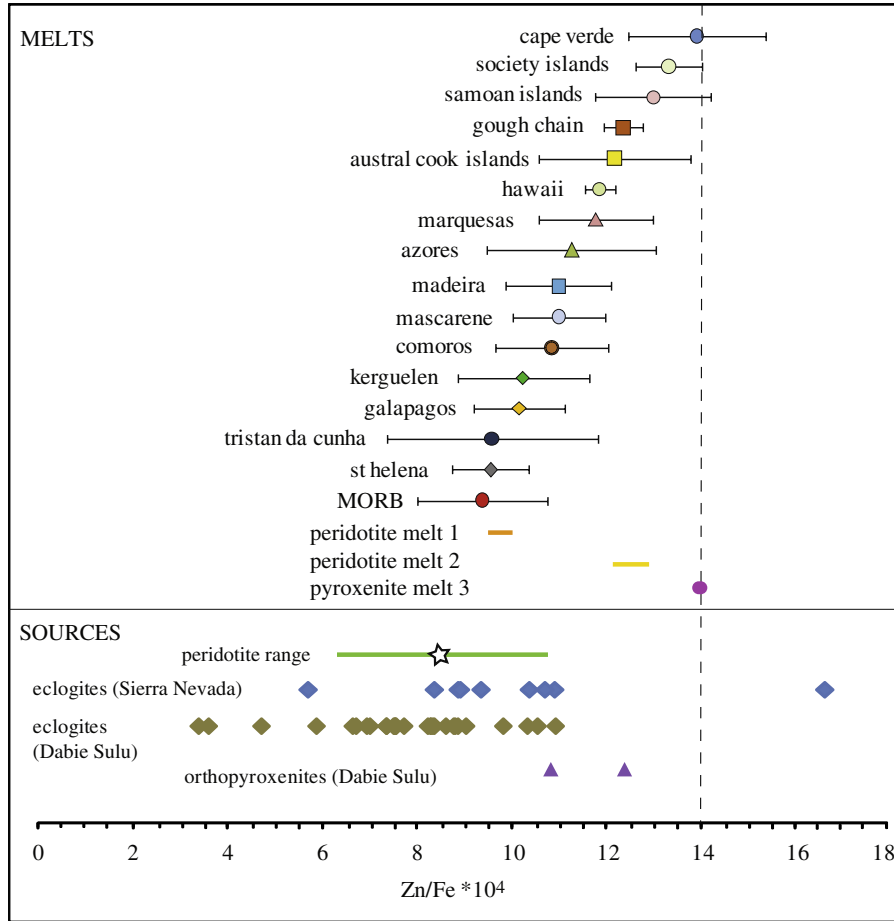
Fig. 6. At the top, Zn/Fe ($\times 10^4$) ratios of MORB and individual OIB suites calculated from their regression lines for MgO wt% = 12 (primitive basalts). Parameters of the regression lines are presented in Table 4. Error bars on Zn/Fe ratios of the melts correspond to the standard error of the predicted Zn/Fe-value for each MgO value in the regression. The white star represents the average Zn/Fe ($\times 10^4$) in peridotites. Peridotite–melt 1 has been calculated using Zn/Fe$_{peridotite}$ = 8.5 and $K_{D(peridotite/melt)}^{Zn/Fe}$ = 0.85–0.9; peridotite melt 2 has been calculated using an extreme peridotite composition with Zn/Fe$_{peridotite}$ = 11 and $K_{D(peridotite/melt)}^{Zn/Fe}$ = 0.85–0.9. Pyroxenite melt three has been calculated using $K_{D(garnet/melt)}^{Zn/Fe} \sim 0.35$ and $K_{D(Cpx/melt)}^{Zn/Fe} \sim 0.7$ from a theoretical 75% Cpx-25% Gt pyroxenite with a Zn/Fe ($\times 10^4$) of 8.5. At the bottom, range of Zn/Fe ($\times 10^4$) ratios of potential sources of oceanic basalts in the mantle. Eclogites Zn/Fe ratios from Dabie Sulu have been compiled from Chavagnac and Jahn (1996), Jahn et al. (1996), Jahn (1998), Zhang et al. (2000) and Liu et al. (2008). Eclogites Zn/Fe ratios from the Sierra Nevada have been compiled from Lee et al. (2006). Orthopyroxenites Zn/Fe ratios have been compiled from Jahn et al. (1996) and Jahn (1998).

peridotite melting can produce the whole range of Zn/Fe variations observed in oceanic basalts. For this, we calculate the predicted Zn/Fe ratios of melts derived from peridotite melting. Because Zn and Fe are slightly incompatible (Doe, 1994) and $K_{D(peridotite/melt)}^{Zn/Fe}$ is slightly less than 1 during mantle melting, the maximum attainable Zn/Fe in a melt derived from peridotite is defined by the limit of zero melting degree and hence given by Zn/Fe$_{melt}$ = Zn/Fe$_{peridotite}$/$K_{D(peridotite/melt)}^{Zn/Fe}$, where Zn/Fe$_{peridotite}$ represents the Zn/Fe ratio of the initial, unmelted peridotite. We adopted the range of $K_{D(peridotite/melt)}^{Zn/Fe}$ obtained from Approach 1 (0.85–0.92), as it was constrained from experimental data. If we then adopt the average Zn/Fe ($\times 10^4$) ratio of ~ 8.5 in peridotites, the maximum Zn/Fe ($\times 10^4$) ratio that can be attained in peridotite-derived melt ranges between 9.3 and 10 (melt 1; Fig. 6). This falls below most of the

primitive OIB data and within error of primitive MORB. If we use the highest extremes of Zn/Fe ($\times 10^4$) observed in peridotites (~ 11), we find Zn/Fe ($\times 10^4$) in the melt to range between 12.2 and 12.9 (melt 2; Fig. 6), which is still below the highest Zn/Fe values found in OIB. Using the K_D's inferred from phenocryst–magma pairs (Approach 2) would lead to even lower Zn/Fe ($\times 10^4$) in the melt. Using the MORB-based exchange coefficient values (Approach 3) yield similar conclusions than Approach 1 (by construct, using K_Ds from Approach 3 must reproduce MORB values). We re-emphasize that these calculated Zn/Fe ratios are strict upper bounds because MORB and OIB represent finite melting degrees. In summary, melts derived from a peridotitic source are predicted to have similar Zn/Fe composition as primitive MORBs, and thus, average peridotite melting fails to reproduce the Zn/Fe compositions of OIBs with high Zn/Fe ratios. Zn/Fe values in OIB are generally

Table 4

Zn/Fe ratios of MORB and OIB predicted for 12% MgO calculated following the equation of their regression line, in the form of Zn/Fe = $a * $MgO + b. Reported error is the standard error of the predicted Zn/Fe-value for each MgO value in the regression.

location	Zn/Fe ($*10^4$) predicted for 12% MgO	Standard error	Regression line parameters	
			a	b
MORI3	9.39	1.37	−0.35	13.63
St. Helena Chain	9.55	0.80	−0.05	10.14
Tristan Da Cunha	9.59	2.22	−0.35	13.80
Galapagos Islands	10.16	0.96	−0.08	11.15
Korguelen	10.24	1.39	−0.04	10.73
Comoros	10.84	1.19	−0.39	15.46
Mascarene Islands	10.99	0.97	−0.07	11.78
Madeira	10.99	1.11	−0.23	13.77
Canary Islands	11.13	2.17	−0.22	13.72
Azores	11.27	1.78	−0.38	15.77
Marquesas	11.78	1.20	−0.02	11.99
Hawaii	11.86	0.32	−0.11	13.14
Austral-Cook Islands	12.18	1.59	−0.29	15.61
Cough Chain	12.36	0.41	−0.21	14.91
Samoan Islands	12.99	1.22	−0.19	15.24
Society Islands	13.31	0.71	−0.07	14.12
Cape Verde Islands	13.91	1.45	−0.07	14.76

too high to be related to partial melting of peridotite mantle only.

4.4.2. Enriched components in the source

The idea that the whole-rock isotopic composition of some oceanic basalts cannot be explained by partial melting of peridotite mantle alone has been suggested by a number of authors (e.g. Hofmann and White, 1982; Hirschmann and Stolper, 1996; Eiler et al., 2000; Humayun et al., 2004; Prytulak and Elliott, 2007; Sobolev et al., 2007). Zn/Fe ratios may help in identifying components that deviate from canonical peridotite mantle. As concluded in the previous sections, high Zn/Fe ratios in primitive magmas are hard to reconcile with melting of a peridotitic mantle alone. Below, we discuss some of the proposed scenarios for major element heterogeneities in OIB source regions, which could explain the high Zn/Fe ratios observed in some OIB localities (e.g. Society Islands, Cape Verde, Samoan Islands; Fig. 6).

Some authors suggest that OIB in part carry a signature of the Earth's liquid outer core, attributing for instance high Fe/Mn ratios to Fe excess associated with core–mantle interactions and the rise of a thermal plume from the core–mantle boundary (Walker et al., 1995; Brandon et al., 1999; Humayun et al., 2004; Qin and Humayun, 2008). Brandon et al. (1999), based on ^{186}Os/^{188}Os anomalies, suggested that the volume of core material involved in core–mantle interactions is at best 1%. Corgne et al. (2008) proposed that there may be up to 30 ppm of Zn in the core. Thus,

any Zn contamination from the core is negligible since lavas contain ∼100 ppm of Zn. As a result, high Zn/Fe ratios observed in some OIB cannot be explained by an excess of Zn. Moreover, an excess in Fe from the core would result in a decrease of the Zn/Fe ratios, which is not seen. It is highly unlikely that high Zn/Fe ratios trace core–mantle interactions.

It is also widely believed that pyroxenites might be present in OIB sources (e.g. Allegre and Turcotte, 1986; Hirschmann et al., 2003; Prytulak and Elliott, 2007; Sobolev et al., 2007; Dasgupta et al., 2010). The exact nature of these pyroxenites is still debated and the question is complex because pyroxenites can form in many different contexts. For instance, it has been suggested that hybrid pyroxenites may form by reaction between eclogite-derived melts and peridotite (Sobolev et al., 2007) and recently, Dasgupta et al. (2010) proposed that carbonated eclogite and volatile-free, silica-excess eclogite may be present in the source of OIB. Such hypotheses are attractive because these lithologies have lower solidus temperatures than peridotites, and hence will melt preferentially, perhaps even in the absence of thermal anomalies like plumes (e.g. Prinzhofer et al., 1989; Hirschmann and Stolper, 1996; Hirschmann et al., 2003; Ito and Mahoney, 2005; Sobolev et al., 2007). However, as stated above, the term "pyroxenite" encompasses rocks that formed in very different contexts: subducted and recycled eclogitic crust, delaminated lower crust, metasomatic veins in the mantle, or melt–rock reaction products (Sobolev et al., 2005). As a consequence, pyroxenites are likely to be characterized by highly variable Zn/Fe ratios. In Fig. 6, we show published Zn/Fe ratios of eclogites and and orthopyroxenites from the Dabie Sulu ultra-high-pressure metamorphic terrane in China (Chavagnac and Jahn, 1996; Jahn et al., 1996; Jahn, 1998; Zhang et al., 2000; Liu et al., 2008) and of garnet pyroxenite xenoliths from late Miocene alkali basalts erupted through the Sierra Nevada batholiths in California, USA (Lee et al., 2006). The Dabie Sulu lithologies most likely have oceanic protoliths, and the Sierra Nevadan pyroxenites represent lower crustal and mantle cumulates associated with arc magmatism. This compilation is by no means exhaustive since we are constrained by the lack of systematic measurements of Zn and Fe in literature studies. It can be seen in Fig. 6 that most of the pyroxenites (including eclogites) have Zn/Fe ratios between 6 and 11, but some approach values as high as 17. If these lithologies were to melt completely, the produced melt would have similar high Zn/Fe ratios to the source, and thus only some pyroxenites will yield high Zn/Fe melts. However, these lithologies are not controlled by olivine and orthopyroxene but rather by pyroxenes or garnet. If $K_D^{Zn/Fe}$ between garnet–melt and clinopyroxene–melt are all <1 as suggested by experiments at 2.9–3.1 GPa and 1325–1390 °C by Pertermann et al. (2004) where $K_{D(garnet/melt)}^{Zn/Fe} \sim 0.35$ and $K_{D(Cpx/melt)}^{Zn/Fe} \sim 0.7$ in MORB-like eclogites, any partial melts of these pyroxenitic lithologies will yield high Zn/Fe ratios. In this case, melts derived from a Gt–Cpx dominated source are likely to display high Zn/Fe ratios, even if the Zn/Fe ratio of the source is similar to peridotites like most recycled eclogites. In Fig. 6, we illustrate this assumption by estimating the composition

of a pyroxenite-derived melt using a 75% Cpx-25% Gt theoretical pyroxenite that has a Zn/Fe ($\times 10^4$) of 8.5. Melts derived from this pyroxenite can reach Zn/Fe ($\times 10^4$) ratios as high as ~14 (melt 3). Any pyroxenite that contains more garnet than what we used in this example would produce melts with even higher Zn/Fe ratios. A more detailed examination of Zn/Fe systematics during pyroxenite melting is beyond the scope of the present paper, but is the topic of one of our current research projects.

Finally, another way to generate high Zn/Fe ratios in the mantle source could be by fluid-metasomatism. Zn enrichment in the mantle source, for instance could occur in arc environments via hydrous fluids released from a subducted slab (Kamenov et al., 2008). Such a scenario could generate high Zn/Fe ratios in the percolated peridotite, which could then yield high Zn/Fe partial melts. However, such melts should display enrichments in fluid-mobile elements, such as Ba, B, Rb, Cs, Cu, Pb, U and light rare-earth elements. Examination of arc basalts would be necessary to assess whether this scenario actually operates on a large scale.

4.5. The role of sulfides

Zn is known to be a fluid-mobile, chalcophile (sulfur-loving) element (e.g. Doe, 1994). Because sulfides are commonly present as accessory phases in peridotites and as hydrothermal sulfides-ores at mid-ocean ridges systems, we discuss here the effect of sulfides on the Zn budget of mafic and ultramafic systems.

Fertile orogenic peridotite contain ~300 ppm S (e.g. Sun, 1982; Lorand, 1989a), mostly in the form of monosulfide solid solution (MSS) and primary sulfides that result from low-temperature subsolidus reequilibration of MSS. Mantle sulfides have modal abundances <1 wt% (e.g. Lorand and Alard, 2001) and Cu–Fe–Ni–S make-up more than 99% of their chemistry (Lorand, 1989b). Thus, sulfides only account for a negligible amount of the Zn budget in peridotite. Moreover, sulfide-silicate melt partition coefficients for Zn are on the order of 1 or less (Shimazaki and Maclean, 1976). It means that Zn is not sufficiently chalcophile to be strongly influenced by sulfides during partial melting.

Finally, Zn is mobilized and concentrated in sulfide deposits at mid-ocean ridges via hydrothermal systems (e.g. Doe, 1994). However, sulfides represent a negligible amount of the whole-rock oceanic crust and are also strongly enriched in elements like Cu and Fe. Thus, it is unlikely that the presence of sulfides modifies significantly the Zn/Fe ratio of recycled oceanic crust.

4.6. Zn/Fe, tracer for oxidation state?

The oxidation state of the Earth's mantle and the processes controlling the oxygen fugacity (fO$_2$) are still debated (Frost and Mccammon, 2008). A pending problem is the lateral variation of upper mantle fO$_2$, particularly beneath arcs in comparison to MORB (Lee et al., 2005; Kelley and Cottrell, 2009; Malaspina et al., 2009; Mallmann and O' Neill, 2009; Rowe et al., 2009). Although constraining fO$_2$ of the mantle is beyond the scope of this paper, we suggest that it may be worth in the near future exploring Zn/Fe

systematics as a possible tracer of Fe oxidation state in melts, which in turn may provide constraints on fO$_2$. An increase in fO$_2$ in the mantle, with all other variables being equal (e.g. modal mineralogy and bulk elemental composition do not change), should lead to the formation of Fe^{3+} at the expense of Fe^{2+}, increasing the Fe^{3+}/Fe^{2+} ratio in the rock without changing its total iron content (Fe$_T$). As stated earlier in this paper, we have implicitly assumed until now that all Fe is in the ferrous state. However, by affecting the Fe^{3+}/Fe^{2+} ratio, fO$_2$ will also modify the exchange partitioning of Zn/Fe$_T$ or Fe$_T$/Mn between peridotite and melt since Fe^{3+} is thought to be more incompatible than Fe^{2+}. Therefore, oxidizing conditions in the mantle should lead to higher Fe^{3+} content in the melt, increasing the total iron content of the melt. This implies that high fO$_2$ peridotitic melts should have low Zn/Fe$_T$ and high Fe$_T$/Mn. As OIB have high Zn/Fe$_T$ and high Fe/Mn$_T$, unusually high fO$_2$ is unlikely to be influencing OIB melting. However, the use of Zn/Fe$_T$ and Fe/Mn$_T$ as tracers for fO$_2$ in the mantle will require careful experimental or theoretical examination of how Zn/Fe partitioning depends on fO$_2$. This is a subject for future work.

5. CONCLUSION

We reported Zn, Mn and Fe systematics in peridotites minerals and whole-rocks as well as in primitive MORBs and OIBs. We showed that Zn/Fe, Zn/Mn and Fe/Mn ratios are minimally fractionated during partial melting of peridotite ($K_{Ds\text{(peridotite/melt)}}$ close to 1). In particular, we showed that Zn/Fe may be a powerful proxy for tracing major element heterogeneities in the Earth's mantle that deviate from a canonical peridotitic composition (olivine and orthopyroxene dominated lithologies). This is because (a) Zn/Fe does not fractionate between olivine, orthopyroxene, and melt, but is strongly fractionated when garnet or clinopyroxene are the dominant phases involved during melting, and (b) Zn/Fe is largely insensitive to olivine fractionation and therefore preserves the signature of the primary magmas, allowing us to put constraints on the composition of the mantle source. Thus, Zn/Fe is unlikely to be affected by modal variations in peridotitic material but will fractionate if garnet and/or clinopyroxene are the main phases in the residue, such as in an eclogite or garnet pyroxenite. These partitioning systematics are confirmed by the similar Zn/Fe ratios in peridotites and primitive MORBs. In contrast, high Zn/Fe ratios of some OIB cannot be explained by peridotite melting only. These high Zn/Fe ratios require, in the source regions of OIBs, lithologies with either high Zn/Fe (some pyroxenites fit this requirement) or more likely garnet–pyroxene rich lithologies that generate high Zn/Fe ratios by fractionation during partial melting. Finally, Zn/Fe ratios hold promise in deciphering large variations of fO$_2$ in the mantle as Zn/Fe systematics should depend on the relative proportions of Fe^{3+} and Fe^{2+}.

REFERENCES

Allegre C. J. and Turcotte D. L. (1986) Implications of a 2-component marble-cake mantle. *Nature* **323**, 123–127.

Bedard J. H. (2005) Partitioning coefficients between olivine and silicate melts. *Lithos* **83**, 394–419.

Bedard J. H. (2007) Trace element partitioning coefficients between silicate melts and orthopyroxene: parameterizations of D variations. *Chem. Geol.* **244**, 263–303.

Bezos A. and Humler E. (2005) The Fe^{3+}/sigma Fe ratios of MORB glasses and their implications for mantle melting. *Geochim. Cosmochim. Acta* **69**, 711–725.

Boyd F. R. (1998) The origin of cratonic peridotites: a major-element approach. *Int. Geol. Rev.* **40**, 755–764.

Brandon A. D., Norman M. D., Walker R. J. and Morgan J. W. (1999) Os-186–Os-187 systematics of Hawaiian picrites. *Earth Planet. Sci. Lett.* **174**, 25–42.

Canil D. (2004) Midly incompatible elements in peridotites and the origins of mantle lithosphere. *Lithos* **77**, 375–393.

Canil D. and O' Neill H. S. C. (1996) Distribution of ferric iron in some upper-mantle assemblages. *J. Petrol.* **37**, 609–635.

Chavagnac V. and Jahn B. (1996) Coesite-bearing eclogites from the Bixiling Complex, Dabie Mountains, China: Sm–Nd ages, geochemical characteristics and tectonic implications. *Chem. Geol.* **133**, 29–51.

Corgne A., Keshav S., Wood B. J., Mcdonough W. F. and Fei Y. W. (2008) Metal-silicate partitioning and constraints on core composition and oxygen fugacity during Earth accretion. *Geochim. Cosmochim. Acta* **72**, 574–589.

Dasgupta R., Jackson M. G. and Lee C.-T. A. (2010) Major element chemistry of ocean island basalts – conditions of mantle melting and heterogeneity of mantle source. *Earth Planet. Sci. Lett.* **289**, 377–392.

Doe B. R. (1994) Zinc, copper, and lead in mid ocean ridge basalts and the source-rock control on Zn/Pb in ocean-ridge hydrothermal deposits. *Geochim. Cosmochim. Acta* **58**, 2215–2223.

Eiler J. M., Schiano P., Kitchen N. and Stolper E. M. (2000) Oxygen-isotope evidence for recycled crust in the sources of mid-ocean-ridge basalts. *Nature* **403**, 530–534.

Embeyisztin A., Scharbert H. G., Dietrich H. and Poultidis H. (1989) Petrology and geochemistry of peridotite xenoliths in alkali basalts from the Transdanubian volcanic region, West Hungary. *J. Petrol.* **30**, 79–105.

Frost D. J. and Mccammon C. A. (2008) The redox state of Earth's mantle. *Annu. Rev. Earth Planet. Sci.* **36**, 389–420.

Gao S., Liu X. M., Yuan H. L., Hattendorf B., Gunther D., Chen L. and Hu S. H. (2002) Determination of forty two major and trace elements in USGS and NIST SRM glasses by laser ablation-inductively coupled plasma-mass spectrometry. *Geostand. Newsl.* **26**, 181–196.

Green D. H., Hibberson W. O. and Jaques A. L. (1979) Petrogenesis of mid-ocean ridge basalts. In *The Earth: Its Origin, Structure and Evolution* (ed. M. W. Maria). Academic Press, London, pp. 265–299.

Hauri E. H. (1996) Major-element variability in the Hawaiian mantle plume. *Nature* **382**, 415–419.

Hirschmann M. M., Kogiso T., Baker M. B. and Stolper E. M. (2003) Alkalic magmas generated by partial melting of garnet pyroxenite. *Geology* **31**, 481–484.

Hirschmann M. M. and Stolper E. M. (1996) A possible role for garnet pyroxenite in the origin of the "garnet signature" in MORB. *Contrib. Mineral. Petrol.* **124**, 185–208.

Hofmann A. W. (1997) Mantle geochemistry: the message from oceanic volcanism. *Nature* **385**, 219–229.

Hofmann A. W. and White W. M. (1982) Mantle plumes from ancient oceanic-crust. *Earth Planet. Sci. Lett.* **57**, 421–436.

Humayun M., Qin L. P. and Norman M. D. (2004) Geochemical evidence for excess iron in the mantle beneath Hawaii. *Science* **306**, 91–94.

Ito G. and Mahoney J. J. (2005) Flow and melting of a heterogeneous mantle: 1. Method and importance to the geochemistry of ocean island and mid-ocean ridge basalts. *Earth Planet. Sci. Lett.* **230**, 29–46.

Jackson M. G. and Dasgupta R. (2008) Compositions of HIMU, EM1, and EM2 from global trends between radiogenic isotopes and major elements in ocean island basalts. *Earth Planet. Sci. Lett.* **276**, 175–186.

Jagoutz E., Palme H., Baddenhausen H., Blum K., Cendales M., Dreibus G., Spettel B., Lorenz V. and Wänke H. (1979) The abundances of major, minor and trace elements in the Earth's mantle as derived from primitive ultramafic nodules. In *Proc. 10th Lunar Planet. Sci. Conf.*

Jahn B. (1998) Geochemical and isotopic characteristics of UHP eclogites and ultramafic rocks of the Dabie orogen: implications for continental subduction and collisional tectonics. In *When continents collide: geodynamics and geochemistry of ultrahigh-pressure rocks*. Kluwer Academic Publ., Dordrecht, pp. 203–239.

Jahn B. M., Cornichet J., Cong B. and Yui T. F. (1996) Ultrahigh-epsilon (Nd) eclogites from an ultrahigh-pressure metamorphic terrane of China. *Chem. Geol.* **127**, 61–79.

Jeffcoate A. B., Elliott T., Kasemann S. A., Ionov D., Cooper K. and Brooker R. (2007) Li isotope fractionation in peridotites and mafic melts. *Geochim. Cosmochim. Acta* **71**, 202–218.

Kamenov G. D., Perfit M. R., Mueller P. A. and Jonasson I. R. (2008) Controls on magmatism in an island arc environment: study of lavas and sub-arc xenoliths from the Tabar-Lihir-Tanga-Feni island chain, Papua New Guinea. *Contrib. Mineral. Petrol.* **155**, 635–656.

Kelemen P. B., Dick H. J. B. and Quick J. E. (1992) Formation of harzburgite by pervasive melt-rock reaction in the upper mantle. *Nature* **358**, 635–641.

Kelemen P. B., Shimizu N. and Salters V. J. M. (1995) Extraction of mid-ocean ridge basalt from the upwelling mantle by focused flow of melt in dunite channels. *Nature* **375**, 747–753.

Kelley K. A. and Cottrell E. (2009) Water and the oxidation state of subduction zone magmas. *Science* **325**, 605–607.

Lassiter J. C. and Hauri E. H. (1998) Osmium-isotope variations in Hawaiian lavas: evidence for recycled oceanic lithosphere in the Hawaiian plume. *Earth Planet. Sci. Lett.* **164**, 483–496.

Le Roux V., Bodinier J. L., Tommasi A., Alard O., Dautria J. M., Vauchez A. and Riches A. J. V. (2007) The Lherz spinel lherzolite: refertilized rather than pristine mantle. *Earth Planet. Sci. Lett.* **259**, 599–612.

Lee C. -T. (2001) The origin, evolution, and demise of continental lithospheric mantle: perspectives from Re–Os isotopes, geochemistry, petrology, and modeling. Ph. D. thesis.

Lee C. -T. and Rudnick R. L. (1999) Compositionally stratified cratonic lithosphere: petrology and geochemistry of peridotite xenoliths from the Labait tuff cone, Tanzania. In *Proceedings of the 7th International Kimberlite Conference* (eds. J. J. G. a. S. R. Richardson). pp. 503–521.

Lee C. T., Rudnick R. L. and Brimhall G. H. (2001) Deep lithospheric dynamics beneath the Sierra Nevada during the Mesozoic and Cenozoic as inferred from xenolith petrology. *Geochem. Geophys. Geosyst.* **2**, 26.

Lee C. T. A. (2005) Trace element evidence for hydrous metaso-matism at the base of the North American lithosphere and possible association with Laramide low-angle subduction. *J. Geol.* **113**, 673–685.

Lee C. T. A., Cheng X. and Horodyskyj U. (2006) The develop-ment and refinement of continental arcs by primary basaltic magmatism, garnet pyroxenite accumulation, basaltic recharge and delamination: insights from the Sierra Nevada, California. *Contrib. Mineral. Petrol.* **151**, 222–242.

Lee C. T. A., Leeman W. P., Canil D. and Li Z. X. A. (2005) Similar V/Sc systematics in MORB and arc basalts: implica-tions for the oxygen fugacities of their mantle source regions. *J. Petrol.* **46**, 2313–2336.

Lee C. T. A., Oka M., Luffi P. and Agranier A. (2008) Internal distribution of Li and B in serpentinites from the Feather River Ophiolite, California, based on laser ablation inductively coupled plasma mass spectrometry. *Geochem. Geophys. Geo-syst.* **9**, 14.

Liu Y. S., Zong K. Q., Kelemen P. B. and Gao S. (2008) Geochemistry and magmatic history of eclogues and ultramafic rocks from the Chinese continental scientific drill hole: subduction and ultrahigh-pressure metamorphism of lower crustal cumulates. *Chem. Geol.* **247**, 133–153.

Longerich H. P., Gunther D. and Jackson S. E. (1996) *Elemental Fractionation in Laser Ablation Inductively Coupled Plasma Mass Spectrometry*. Springer Verlag.

Lorand J.-P. and Alard O. (2001) Platinum-group element abun-dances in the upper mantle: new constraints from in situ and whole-rock analyses of Massif Central xenoliths (France). *Geochim. Cosmochim. Acta* **65**, 2789–2806.

Lorand J. P. (1989a) Abundance and distribution of Cu–Fe–Ni sulfides, sulfur, copper and platinum-group elements in oro-genic-type spinel lherzolite massifs of Ariege (Northeastern Pyrenees, France). *Earth Planet. Sci. Lett.* **93**, 50–64.

Lorand J. P. (1989b) Mineralogy and chemistry of Cu–Fe–Ni sulfides in orogenic-type spinel peridotite bodies from Ariege (Northeastern Pyrenees, France). *Contrib. Mineral. Petrol.* **103**, 335–345.

Lyubetskaya T. and Korenaga J. (2007) Chemical composition of Earth's primitive mantle and its variance: 2. Implications for global geodynamics. *J. Geophys. Res. Solid Earth* **112**, 15.

Malaspina N., Poli S. and Fumagalli P. (2009) The oxidation state of metasomatized mantle wedge: insights from C–O–H-bearing garnet peridotite. *J. Petrol.* **50**, 1533–1552.

Mallmann G. and O' Neill H. C. (2009) The crystal/melt partitioning of V during mantle melting as a function of oxygen fugacity compared with some other elements (Al, P, Ca, Sc, Ti, Cr, Fe, Ga, Y, Zr and Nb). *J. Petrol.* **50**, 1765–1794.

Mcdonough W. F. and Sun S.-S. (1995) The composition of the Earth. *Chem. Geol.* **120**, 223–253.

Meagher E. P. (1982) Silicate garnets. In *Orthosilicates: Reviews in Mineralogy*, vol. 5, second ed (ed. P. H. Ribbe). Mineral Soc. America, Washington, DC, pp. 25–66.

Menzies M. A., Rogers N., Tindle A. and Hawkesworth C. J. (1987) Metasomatic and enrichment processes in lithospheric peridotites, an effect of asthenosphere–lithosphere interaction. In *Mantle Metasomatism* (eds. M. A. Menzies and C. J. Hawkesworth). Academic Press, London, pp. 313–361.

Muntener O., Pettke T., Desmurs L., Meier M. and Schaltegger U. (2004) Refertilization of mantle peridotite in embryonic ocean basins: trace element and Nd isotopic evidence and implications for crust-mantle relationships. *Earth Planet. Sci. Lett.* **221**, 293–308.

Norman M., Garcia M. O. and Pietruszka A. J. (2005) Trace-element distribution coefficients for pyroxenes, plagioclase, and olivine in evolved tholeites from the 1955 eruption of Kilauea

Volcano, Hawai'i, and petrogenesis of differentiated rift-zone lavas. *Am. Miner.* **90**, 888–899.

Oreilly S. Y., Griffin W. L. and Ryan C. G. (1991) Residence of trace elements in metasomatized spinel lherzolite xenoliths – a proton-microprobe study. *Contrib. Mineral. Petrol.* **109**, 98–113.

Palme H. and O'neill H. S. C. (2003) Cosmochemical estimates of mantle composition. In *Treatise on Geochemistry – The Mantle and Core* (ed. R. W. Carlson). Elsevier, pp. 1–38.

Pertermann M., Hirschmann M. M., Hametner K., Gunther D. and Schmidt M. W. (2004) Experimental determination of trace element partitioning between garnet and silica-rich liquid during anhydrous partial melting of MORB-like eclogite. *Geochem. Geophys. Geosyst.* **5**, 23.

Pilet S., Baker M. B. and Stolper E. M. (2008) Metasomatized lithosphere and the origin of alkaline lavas. *Science* **320**, 916–919.

Prinzhofer A., Lewin E. and Allegre C. J. (1989) Stochastic melting of the marble cake mantle – evidence from local study of the East Pacific rise at 12-degrees-50′N. *Earth Planet. Sci. Lett.* **92**, 189–206.

Prytulak J. and Elliott T. (2007) TiO$_2$ enrichment in ocean island basalts. *Earth Planet. Sci. Lett.* **263**, 388–403.

Putirka K. D. (2005) Mantle potential temperatures at Hawaii, Iceland, and the mid-ocean ridge system, as inferred from olivine phenocrysts: evidence for thermally driven mantle plumes. *Geochem. Geophys. Geosyst.* **6**, 14.

Qi Q., Taylor L. A. and Zhou X. M. (1995) Petrology and geochemistry of mantle peridotite xenoliths from SE China. *J. Petrol.* **36**, 55–79.

Qin L. P. and Humayun M. (2008) The Fe/Mn ratio in MORB and OIB determined by ICP-MS. *Geochim. Cosmochim. Acta* **72**, 1660–1677.

Rampone E., Piccardo G. B., Vannucci R. and Bottazzi P. (1997) Chemistry and origin of trapped melts in ophiolitic peridotites. *Geochim. Cosmochim. Acta* **61**, 4557–4569.

Ramsay W. R. H., Crawford A. J. and Foden J. D. (1984) Field settings, mineralogy, chemistry, and genesis of arc picrites, New-Georgia, Solomon-Islands. *Contrib. Mineral. Petrol.* **88**, 386–402.

Roeder P. L. and Emslie R. F. (1970) Olivine-liquid equilibrium. *Contrib. Mineral. Petrol.* **29**, 275–289.

Rowe M. C., Kent A. J. R. and Nielsen R. L. (2009) Subduction influence on oxygen fugacity and trace and volatile elements in basalts across the cascade volcanic arc. *J. Petrol.* **50**, 61–91.

Ruzicka A., Snyder G. A. and Taylor L. A. (2001) Comparative geochemistry of basalts from the Moon, Earth, HED asteroid, and Mars: implications for the origin of the Moon. *Geochim. Cosmochim. Acta* **65**, 979–997.

Salters V. J. M. and Dick H. J. B. (2002) Mineralogy of the mid-ocean-ridge basalt source from neodymium isotopic composi-tion of abyssal peridotites. *Nature* **418**, 68–72.

Shimazaki H. and Maclean W. H. (1976) Experimental study on partition of Zinc and Lead between silicate and sulfide liquids. *Miner. Depos.* **11**, 125–132.

Simon N. S. C., Irvine G. J., Davies G. R., Pearson D. G. and Carlson R. W. (2003) *The Origin of Garnet and Clinopyroxene in "Depleted" Kaapvaal Peridotites*. Elsevier Science BV.

Sobolev A. V., Hofmann A. W., Kuzmin D. V., Yaxley G. M., Arndt N. T., Chung S. L., Danyushevsky L. V., Elliott T., Frey F. A., Garcia M. O., Gurenko A. A., Kamenetsky V. S., Kerr A. C., Krivolutskaya N. A., Matvienkov V. V., Nikogosian I. K., Rocholl A., Sigurdsson I. A., Sushchevskaya N. M. and Teklay M. (2007) The amount of recycled crust in sources of mantle-derived melts. *Science* **316**, 412–417.

Sobolev A. V., Hofmann A. W., Sobolev S. V. and Nikogosian I. K. (2005) An olivine-free mantle source of Hawaiian shield basalts. *Nature* **434**, 590–597.

Sun S. S. (1982) Chemical composition and origin of the Earth's primitive mantle. *Geochim. Cosmochim. Acta* **46**, 179–192.

Vaselli O., Downes H., Thirlwall M., Dobosi G., Coradossi N., Seghedi I., Szakacs A. and Vannucci R. (1995) Ultramafic xenoliths in Plipleistocene alkali basalts from the Eastern Transylvanian basin – depleted mantle enriched by vein metasomatism. *J. Petrol.* **36**, 23–53.

Walker R. J., Morgan J. W. and Horan M. F. (1995) Os-187 enrichment in some plumes – evidence for core–mantle interaction. *Science* **269**, 819–822.

Walter M. J. (1998) Melting of garnet peridotite and the origin of komatiite and depleted lithosphere. *J. Petrol.* **39**, 29–60.

Walter M. J. (2003) Melt extraction and compositional variability in mantle lithosphere. In *Treatise on Geochemistry – The Mantle and Core* (ed. R. W. Carlson). Elsevier-Pergamon, Oxford, pp. 363–394.

Workman R. K. and Hart S. R. (2005) Major and trace element composition of the depleted MORB mantle (DMM). *Earth Planet. Sci. Lett.* **231**, 53–72.

Zhang Z. M., Xu Z. Q. and Xu H. F. (2000) *Petrology of Ultrahigh-Pressure Eclogites from the ZK703 Drillhole in the Donghai, Eastern China*. Elsevier Science BV.

Zindler A. and Hart S. (1986) Chemical geodynamics. *Annu. Rev. Earth Planet. Sci.* **14**, 493–571.

Associate editor: Edward M. Ripley